LAPPEENRANTA-LAHTI UNIVERSITY OF TECHNOLOGY LUT

School of Engineering Science

Chemical Engineering

Mikko Aalto

Modelling of Ion exchange Process in Purification of Lithium-ion Battery Leachates

Supervisors: Prof. Tuomo Sainio

D.Sc Sami Virolainen

Abstract

Lappeenranta-Lahti University of Technology LUT

School of Engineering Science

Chemical Engineering

Mikko Aalto

Modelling of Ion exchange Process in Purification of Lithium-ion Battery Leachates

Master's thesis

2021

72 pages, 23 figures and 1 table

Examiners: Prof. Tuomo Sainio

D.Sc Sami Virolainen

Keywords: lithium-ion battery, ion exchange, modelling, NICA, ion exchange equilibrium, simulation, ion exchange kinetics

Because of the increased use of electrical devices, the use of lithium-ion batteries has increased. To combat the skyrocketing increase in demand for the metals used in these batteries, different types of processes have been studied for recycling purposes. Ion exchange utilizing chelating resins has risen as a potential solution due to their good selectivity for the metals that are present in lithium-ion batteries.

Simulations provide great insight on different types of processes. For the ion exchange process, different types of methods were studied to find the most suitable one for simulating ion exchange processes for lithium-ion battery leachate. Out of the mechanistic models to describe ion exchange equilibrium, non-ideal competitive adsorption NICA was found to be the most suitable for this type of multicomponent ion exchange process.

The parameters in the NICA model were fitted visually to match previously conducted loading and elution experiments. Achieving an accurate model for such a complex process proved to be very difficult because of the high amount of metals in the process and the lack of more in depth experimental data. However, the simulation results showcased generally good fits for the loading step of the ion exchange process. The understanding about simulating multicomponent ion exchange processes gained during this thesis can be applied when planning subsequent research utilizing simulations.

Tiivistelmä

Lappeenrannan-Lahden Teknillinen Yliopisto LUT

School of Engineering Science

Chemical Engineering

Mikko Aalto

Ioninvaihtoprosessin mallinnus litiumioniakkujätteen kierrätyksessä

Diplomityö

2021

72 sivua, 23 kuvaa ja 1 taulukko

Tarkastajat: Prof. Tuomo Sainio

D.Sc Sami Virolainen

Avainsanat: litiumioniakku, ioninvaihto, mallinnus, NICA, ioninvaihto tasapaino, simulaatio, ioninvaihto kinetiikka

Elektronisten laitteiden käytön lisääntyessä myös litiumioniakkujen käyttö on lisääntynyt. Akuissa käytettävien metallien lisääntyvä käyttö on lisännyt painetta tutkia erilaisia menetelmiä akkujätteen kierrätykselle. Ioninvaihto käyttäen kaltoivia hartseja on noussut yhdeksi potentiaaliseksi vaihtoehdoksi. Kelatoivat hartsit ovat hyvin selektiivisiä litiumioniakuissa oleville metalleille.

Prosessien simuloiminen on hyödyllinen työkalu, kun halutaan lisätä ymmärrystä tietyistä prosesseista. Monia erityyppisiä malleja tutkittiin löytääkseen ioninvaihtoprosessille sopivin. Kaikista mekaanisista malleista, jotka kuvaavat ioninvaihdon tasapainotilaa, epäideaalinen kilpaileva adsorptio NICA osoittautui potentiaalisimmaksi vaihtoehdoksi monikomponenttiselle ioninvaihtoprosessille.

NICA-mallissa olevat parametrit sovitettiin visuaalisesti olemassa olevaan ioninvaihtoprosessin lataus- ja eluutiovaiheen koedataan. Tarkan mallin simulointi monimutkaiselle prosessille oli kuitenkin todella haasteellista. Eniten haasteita tuottivat metallien suuri määrä ja koedatan vähäisyys. Kuitenkin ioninvaihtoprosessin latausvaiheessa saavutettiin hyviä tarkkuuksia liuoksessa oleville metalleille. Tutkimuksesta saatujen tietojen avulla, voidaan paremmin ymmärtää ja suunnitella simulaatioita käyttäviä tulevia monikomponenttisia ioninvaihtoprosesseja sisältäviä tutkimuksia.

Foreword

This master's thesis was a part of a larger overall study and it was done between May 2020 and May 2021 in the Department of Separation Science at Lappeenranta-Lahti University of Technology at LUT School of Engineering Science.

First, I would like to thank Tuomo Sainio and Sami Virolainen for being a part of this thesis. Both provided me with superb information that without, I would have never been able to get even this far. They were also super kind even when I was struggling with motivation during the making of this thesis.

I would also like to thank the whole staff at the department of Chemical Engineering at LUT university. Your guidance and teachings provided me with vast array of information from the world known as chemistry. You also gave me confidence to continue into the job market because of your high standard of teaching.

Lastly huge thanks to every one of my colleague students. You helped me through this mountain of a task. We shared some amazing moments and memories that I will cherish the rest of my life. I moved here to Lappeenranta just for studies, but after six years I can comfortably call this place home.

Show must go on.

7th of May 2021

Mikko Aalto

TABLE OF CONTENTS

LIST OF SYMBOLS

a	activity, -
a_{min}	Approximated minimum distance between ions, m
A	surface area, m^2
A_γ	Debye-Hückel constant, -
B	second virial coefficient, L/mol
B_{SCM}	abbreviation, -
c	concentration, mol/L
C	capacitance, F/m^2
C_{ij}	Pitzer model parameter
D	mutual diffusion coefficient, cm^2s^{-1}
D_L	apparent dispersion coefficient, cm^2s^{-1}
D_p	pore diffusivity, cm^2s^{-1}
D_s	surface diffusivity, cm^2s^{-1}
e	electron charge, C
E^0	cell potential, V
F	Faraday constant, C/mol
F_{DH}	contribution of Debye-Hückel model, -
h	NICA parameter, -
ΔH_{ads}	adsorption enthalpy, J/mol
I	ionic strength, mol/kg or mol/L
J	diffusion flux, $mol/(m^2s)$
k	mass transport coefficient, m/s
k_B	Boltzmann's constant, J/K
k_f	Freundlich constant, -
K_{AB}	thermodynamic equilibrium constant, -
K_{aB}	corrected selectivity coefficient, -

K_c	selectivity coefficient, -
m	molal concentration, mol/kg
m_{SCM}	surface complexation model parameter, -
n	amount of substance, mol
N	mole flux, mol/(m^{2}s)
N_0	Avogadro's constant, mol^{-1}
p	NICA parameter, -
q	amount bound to solid phase, mol/kg
q^{max}	total amount of sorption sites, mol/kg
q^*	equilibrium concentration of the resin, mol/kg
Q	generalized separation factor, -
r	radial coordinate of spherical symmetry, -
R	ideal gas constant, J/Kmol
R_s	radius, m
s	distance to symmetry plane, cm
t	time, s
T	temperature, K
u	interstitial velocity, m/s
V	electric potential, C
y	mole fractions, mol
$y(X)$	dimensionless loading of ions X, -
z	ion charge, -
z_c	axial coordinate of the column, -

Greek Letters

α	dissociation degree, -
β	Pitzer model parameter, -
β_{DH}	abbreviation for Debye-Hückel model, -
γ	activity coefficient, -

ε	porosity, -
ε_p	internal porosity, -
Θ	cation-cation interactions, -
κ	NICA selectivity coefficient, L/mol
Λ	Wilson model parameter, -
μ	chemical potential, J/kg or J/mol
v	molar volume, m^3/mol
ρ	density, kg/m^3
Ψ	cation-anion-cation interactions, -
ω	fraction of sites, -

Subscripts

0	initial value
ext	external
i, j	component
k	site population
s	solvent

Abbreviations

GRM	General rate model
H	proton
LDF	Linear driving force
LIB	Lithium ion battery
M	metal cation
NICA	Non-ideal competitive adsorption
SCM	Surface complexation model

1 Introduction

Lithium-ion batteries (LIBs) have been the dominant power source for portable electronic devices since the early 1990's (Chagnes and Pospiech, 2013). Recently, lithium-ion batteries have also become the most potential solution for the transportation sector, regarding the use of fossil fuels (Kushnir, 2015). The rising demand for lithium-ion batteries have caused concern about the availability of the metals used to assemble these batteries. The sources of lithium are unlikely to strain due to the growing automotive market, but in the case of cobalt, the concerns and price increase has caused manufacturers to drift towards nickel (Gaines, 2018)

Because of the rapid growth of demand for lithium-ion batteries, their recycling has become a viable option as an additional source for nickel, lithium and cobalt. Secondly, sustainability and the growth of environmental values generate more demand for battery recycling, especially because lithium-ion batteries contain hazardous materials. (Chagnes and Pospiech, 2013) Due to this, the possibilities of recycling have been largely researched on as a solution to rising prices, demand, reducing costs of disposal. (Gaines, 2018)

The battery recycling processes can be divided into hydrometallurgical processes and pyrometallurgical processes (Georgi-Maschler et al., 2012). Due to the high selectivity, efficiency and limited waste generation, hydrometallurgical processes are considered to be more sustainable. In the hydrometallurgical processes, acid leaching is an indispensable step, and it can be considered as a pretreatment step. After leaching, the most common procedures are solvent extraction and chemical precipitation. (Zhang et al., 2013) Ion exchange is somewhat overlooked in this manner as it shows potential as a good way of separating metals from the leachate. The purpose of this thesis is to gain an understanding about different types of models and compare their applicability to simulate ion exchange for lithium-ion battery leachate. This helps to understand the occurring phenomena in a multicomponent ion exchange system. With this understanding and a suitable model for predicting behavior in the system, ion exchange could become a more used and viable option in the recycling processes.

2. Composition of Lithium-ion Batteries

The lithium-ion battery structure is more complex than other main types of batteries, such as Ni-Cd or Pb-acid batteries, because of the need of different compositions in order to produce high energy densities. (Zhang et al., 2013) Because of this reason, it is difficult to specify the exact composition of the large amounts of battery scraps that can be assembled. Lithium-ion batteries have a lot of valuable metals in metallic form and as inorganic metallic components. The interesting metals regarding this paper, are contained as the cathode material inside LIBs. (Georgi-Maschler et al., 2012) The cathode contains lithium metal oxides. The most common of these cathode materials are $LiMn_2O_4$, $LiCoO_2$, $LiNiO_2$ and $LiFePO_4$. (Zhang et al., 2013) The cathode is linked with polyvinylidene fluoride (PVDF) (Golmohammadzadeh et al., 2017). Other metals like aluminum (Al) and copper (Cu) are used as foil materials for the anode and cathode inside LIBs. The anode itself is usually graphite. (Ku et al., 2016)

2.1 Valuable Metals of Lithium-ion Batteries

Because the valuable metals are present in the cathode materials and electrolytes in LIBs, their recovery is the biggest driving force for recycling, since it makes the process economically attractive. Metals like cobalt and possibly lithium need to be recovered especially in the case of cobalt, since it has many military and industrial uses. Due to cobalt's availability being lower than most transition metals, it is almost 3 times as expensive as nickel and almost 6 times as expensive as copper ("London Metal Exchange: Home," 2020). In the case for lithium, the increasing demand of batteries, especially into the automobile industry, the increasing demand of production can be helped by recycling lithium from used batteries. Also, the vast majority of lithium is concentrated in South America, which can cause geopolitical risks for lithium accessibility. (Chagnes and Pospiech, 2013)

There are other incentives to recycle LIBs than just it being economically attractive. For example, cobalt and nickel are known health hazards. Nickel and cobalt are classified as carcinogenic, mutagenic and reprotoxic (CMR) substances. At high temperatures, the mix of organic and inorganic compounds possess a risk for explosion and pollution. The regulations of governments

can increase the amount of interest in LIB recycling. However, if the recycling process is not economically feasible, the costs of recycling may be included in battery prices. (Chagnes and Pospiech, 2013)

2.2 Acid Leaching

Acid leaching is an indispensable part of the hydrometallurgical processes where the metals are transferred from solids to aqueous solutions (Gao et al., 2018). Common acids used in acid leaching of LIBs are sulfuric acid (H_2SO_4) (Pagnanelli et al., 2017), nitric acid (HNO_3) (Gao et al., 2018), hydrochloride acid (HCl) (Guo et al., 2016) as well as some organic acids such as citric acid, oxalic acid and malic acid. The problem with strong inorganic acids are the harmful gases SO_3, NO_x and Cl_2 generated in the leaching process. (Golmohammadzadeh et al., 2017) Extremely high efficiencies can be reached with acid leaching. The maximum efficiencies can reach over 99%. (Guo et al., 2016)

2.3 Effect of Hydrogen Peroxide in Acid Leaching

Hydrogen peroxide H_2O_2 is widely used as a strong oxidant in acid leaching of LIBs. H_2O_2 increases the dissolution of the valuable metals such as Cu, Li, Co, Mn and Ni in the leaching process. (Li et al., 2017) For example, the bond generated between oxygen and cobalt is very strong. That makes leaching of such compounds difficult. (Chagnes and Pospiech, 2013) The function of H_2O_2 is to convert metals from their higher valence to lower valences (Gao et al., 2018). The conversion from higher valence to lower valence in the case of cobalt are as follows (Golmohammadzadeh et al., 2017):

$$H_2O_2 + 2H^+ + 2e^- \leftrightarrow 2H_2O \quad E^0 = +1.78V \tag{1}$$

$$Co^{3+} + e^- \leftrightarrow Co^{2+} \quad E^0 = +1.8V \tag{2}$$

3. Ion Exchange

Ion exchange processes always include mobile ions that are in a solution, that bound to a solid matrix. The solid matrix contains functional groups that are capable of binding the desired ions. (Inglezakis and Zorpas, 2012) Ion exchange is a growing technology in multiple chemical industries. However, it requires deep understanding of the principles to be implemented correctly. When used correctly, ion exchange can remove all desired atoms from a solution. Therefore, ion exchange can be used for small concentration of metals for water treatment as well as large-scale removal of metals in metal finishing and hydrometallurgy. (Nasef and Ujang, 2012)

The basis of ion exchange is that the exchangers can be considered as solid electrolytes that are able to exchange ions in a solution with other ions possessing the same charge (Lito et al., 2012). There are several known causes, why some ionic species are preferred over another by the ion exchanger. These causes can be electrostatic interactions between the charged species and the counter ions. The preference can also be caused by other interactions between ions and by the pore size of the exchanger being too small to some large ions. (Helfferich, 1995) The exchanger resins can be grouped into anion exchanges and cation exchanger based on, if the solid resin contains mobile cations H^+ or mobile anions Cl^-. (Lito et al., 2012)

Ion exchange is quite similar with adsorption. In both adsorption and ion exchange there is mass transport occurring from liquid to solid phase. The mass transport happens via diffusion. However, there are some key differences that differentiate ion exchange from basic adsorption processes. One of the biggest differences is that in ion exchange, the sorbed species is an ion, whereas in adsorption the species is a neutral compound. Another key difference is that in ion exchange, a counterion replaces the adsorbed ion in the solution. This type of two-way traffic does not take place in diffusion. The electroneutrality principle dictates that the exchange of ions must happen so that the total charge of the sorbed and desorbed species stay neutral. Even when there are several key differences between the two processes, most of the mathematical models used to simulate ion exchange phenomena were initially developed for adsorption processes. (Inglezakis and Zorpas, 2012)

LIBs are recycled by combined processes utilizing many different technologies. The most common ones are crushing, acid leaching, chemical precipitation and solvent extraction. (Zhang et al., 2013)

Even though ion exchange showcases a lot of possibilities in LIB recycling, it has been somewhat overlooked as a possible process for recycling LIBs.

3.1 Ion Exchange Resins

Ion exchange resins are functional compounds that can be classified in various ways. They can be classified by their physical form, material origin, chemical function and the nature of the fixed group. The material origin of the resin can be a synthetic organic polymer that can function as a cation or an anion exchanger. Natural ion exchangers, such as zeolites, act only as cation exchangers. Different physical forms of ion exchangers are various types of resins and beads, membranes, hydrogels and fibers. (Nasef and Ujang, 2012)

Because of the similarities of ion exchange resins and conventional acids and bases, the resins can also be classified as weakly acidic, weakly basic, strongly acidic and strongly basic. Strong acid exchangers contain sulfonate groups ($-SO_3^-$). These strong acid exchangers can function in all pH ranges, while weak acidic exchangers with carboxyl groups ($-COO^-$) stop being active below 4-6 pH. Strong and weak basic exchangers act similarly. Strong basic exchangers function in all pH ranges when, while weak basic exchangers are not active in high pH values. (Nasef and Ujang, 2012)

In terms of physical attributes, ion exchange beads can either have a multichannel structure making them macroporous, or they can possess a dense structure with no pores making them microporous. The selection of macro- or microporous ion exchanger is entirely dependent on the application. Macroporous resins are able to catch larger ions, whereas microporous resins are less fragile. (Nasef and Ujang, 2012)

In according to (Nasef and Ujang, 2012) there are eight desired properties in every ion exchange resins for them to be industrially applicable. They are dependent on the chemical and physical properties of the ion exchanger. The eight proposed eight properties are chemical stability, hydrophilic structure, cross-linking, fast kinetics, consistent particle size, surface area, physical stability and ion exchange capacity.

3.2 Chelating Resins

Chelating resins are a subgroup of traditional resins. Chelating resins are insoluble in water because of their stability providing polymer matrix and their functional groups that cause metal complexation. (Nasef and Ujang, 2012) Chelating resins have been developed to provide sensitivity and high selectivity especially for heavy transition metals. Ion exchange processes utilizing traditional ion exchange resins for separation of metals such as cobalt, lithium, manganese, nickel and copper can have negative effects on the process when very alkali metal salts are present in the solution. The presence of these metal salts could lower the column capacity by swamping the column and degrading the separation of cations. Because of this reason, highly selective chelating ion exchange resins have been developed to prevent these shortcomings. (Sud, 2012)

The premise of chelating resins is the complexation of metals, that have ring-type structures that have a covalent coordinate bond with the functional groups on the surface of the chelating resin. The binding happens between multiple donor atoms present in the chelating ligand. The ligand itself is neutral, and it forms charged complexes with metal ions. With the case of transition metals, the formed complexes are stable (Laatikainen et al., 2012). The chelating ligands have strong affinity to hydrogen ions (OH^-). Some example of chelating ligands can be seen in Figure 1.

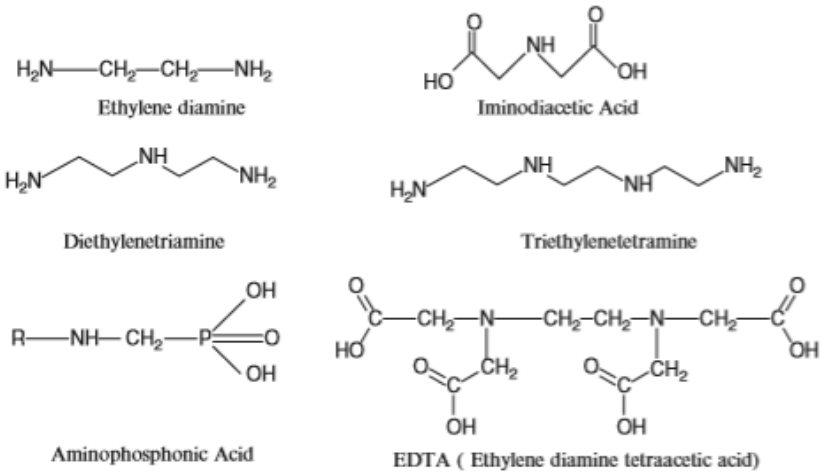

Figure 1. Chelating ligands (Sud, 2012)

Higher H^+ concentrations in the solution weaken the chelates by speeding up elution. Because of this, acidic eluents are utilized for controlling the equilibrium. Temperature and pH also play a key role in the separation of desired metal ions. The equilibrium between a metal ion and a chelating resin can be written as follows: (Sud, 2012)

$$M^{2+} + 2RL^{-}H^{+} \rightleftharpoons (RL)_2M + 2H^{+} \quad (3)$$

where M^{2+} metal ion

$RL^{-}H^{+}$ chelating resin

4. Ion Exchange Equilibrium

Modeling and simulation are important steps for determining dynamic behavior and optimizing operation conditions. It is crucial to understand the basic principles of any process in order to achieve an accurate model, that can be used to predict behavior. (Aniceto et al., 2012) In the case of ion exchange, the modelling of equilibrium and kinetics is crucial for simulations. The equilibrium is commonly represented as an ion exchange isotherm. This isotherm showcases the concentrations of counter ions in the ion exchange resin as a function of their concentration in the ion exchange solution. Experimental data is needed to validate the generated model. However, the models and simulations are more useful, when they can predict behavior of a process with different conditions than the ones used in the experimental data. (Lito et al., 2012)

With the case of the LIB leachate, it is important to establish an understanding of the ion exchange equilibria in the system. The models used to determine the activity coefficients should consider that the ion exchange process for LIB leachate is a multicomponent non-ideal system. The different metal ions present in the LIB leachate have different charges. The model also should take into consideration that the different ions compete with the same sorption sites in the resin.

4.1 Modelling Principles

The objective of the model is to predict behavior in the targeted system. For ion exchange, it means predicting the movement of each component inside either batch reactors or fixed bed columns. This also gives an idea of when the resin has reached its limit and needs to be regenerated or changed. The parameters that are evaluated in the model are fitted to represent real life situations. Shallcross et al. (2003) specified critical criteria for parameters in different multicomponent models. The parameters need to be independent of the concentrations in the solution phase. The model needs to be consistent throughout the whole process. This is because multicomponent systems are usually complicated. The mathematical models have more equations than unknown parameters. (Provis et al., 2005)

After fitting the parameters accurately, the main objective is to accurately describe the equilibrium position for each component in the system. From the results of the model, the behavior of each compound in the system and the effects of conditions can be accurately predict without expensive analysis. (Provis et al., 2005)

4.1.1 Breakthrough Curve

Breakthrough curves and concentration profiles are the most essential tool of showcasing the results of using the chosen model and evaluating the parameters. Breakthrough curves showcase the movement of the mass transfer zone that occurs in the process column. The mass transfer zone moves in the graphical representation based on the exhaustion of the adsorbent in the column. The breakpoint is usually considered to be the moment when the ratio between inlet and outlet concentrations of a specific compound is 0.05. The operating limit of the column is reached when the ratio jumps up to 0.90. The basic characteristics of a breakthrough curve is showcased in Figure 2. (Chowdhury et al., 2014)

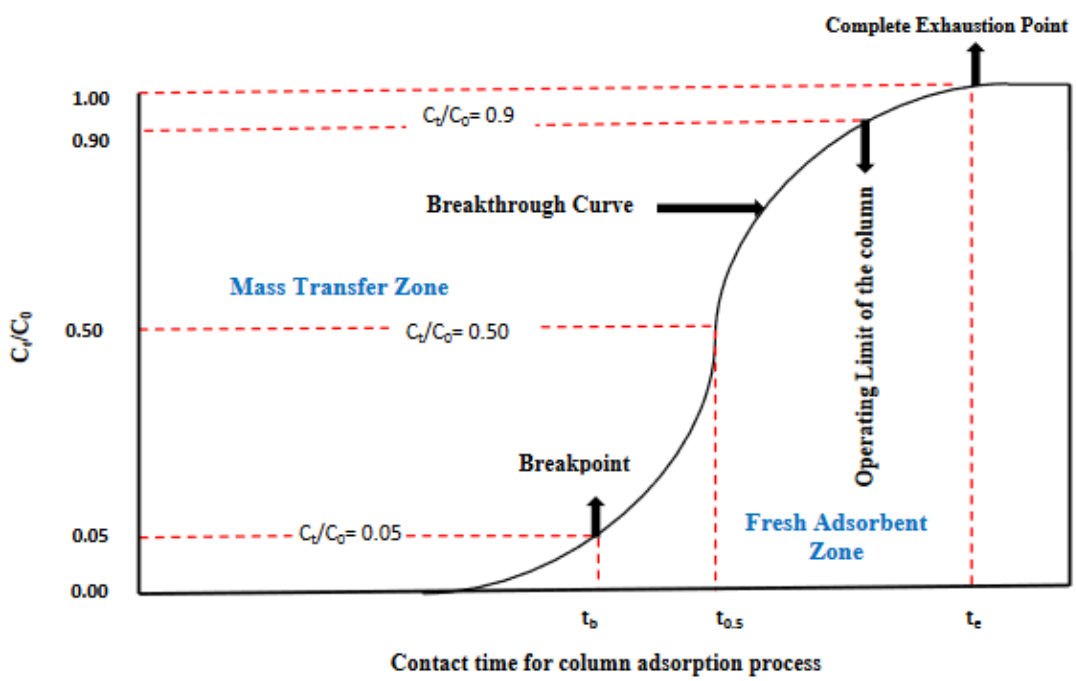

Figure 2. Overview of principal characteristics of a breakthrough curve in a fixed bed column process. (Chowdhury et al., 2014)

Breakthrough curves are not only affected by the parameters of the model used. Initial operation conditions have significant effects on the breakthrough curves. Influent concentrations, bed height and influent rate have effects on the time when the breakthrough occurs. When using a smaller bed height, larger flow rates and concentrations, the adsorbent is exhausted quicker and the breakthrough curve is shifted to the left. (Chowdhury et al., 2014)

4.2 Basic Thermodynamic Framework

A popular approach to represent the exchange of ion between the solution and exchanger phase is to treat ion exchange as a chemical reaction (Vo and Shallcross, 2003). This approach is called "Homogenous Mass Action Models", because the ion exchanger is thought to be homogenous, while the nonidealities of the solution and solid phase are accounted in the activity coefficients (Lito et al., 2012). The exchange of ions A^{za} and B^{zb} with valences z_a and z_b is described with the following equation: (Vo and Shallcross, 2003)

$$z_b A^{\pm z_a} + \overline{z_a B^{\pm z_b}} \leftrightarrow \overline{z_b A^{\pm z_a}} + z_a B^{\pm z_b} \tag{4.1}$$

where the top bar represents the solid phases. With this stoichiometric approach, electroneutrality can be ensured in the process.

Important concept to ion exchange thermodynamics is the chemical potential of the species. For ion exchange processes specifically, the determining the chemical potentials of the different species in the solid phase. The equation that relates the chemical potential μ with concentration can be written as: (Soldatov, 1995)

$$\mu_i = \mu_i^0 + RTlnc_i + RTln\gamma_i \tag{4.2}$$

$$= \mu_i^0 + RTlna_i$$

where γ is the activity coefficient of species i, a is activity, R represents ideal gas constant, c is concentration, T is temperature and μ_i^0 represents the standard chemical potential. The stoichiometry in Eq. (4.1) can be written with chemical potentials as follows: (Ioannidis et al., 2000)

$$z_b\mu_A + \overline{z_a\mu_B} \leftrightarrow \overline{z_b\mu_A} + z_a\mu_B \tag{4.3}$$

It is very important to establish a condition for the equilibrium of the ion exchange process. This can be done by following the energy minimum condition for Gibbs energy. (Soldatov, 1995)

$$\overline{\mu_A}d\overline{n_A} + \overline{\mu_B}d\overline{n_B} + \overline{\mu_s}d\overline{n_s} + \mu_A dn_A + \mu_B dn_B + \mu_s dn_s = 0 \tag{4.4}$$

where n is the number of moles of the species. The top bars represent the solid phase and the subscript s is the solvent. In order to secure mass balances and electrical neutrality in the system: (Soldatov, 1995)

$$d\overline{n_A} = dn_A,\ d\overline{n_B} = dn_B,\ d\overline{n_s} = dn_s \tag{4.5}$$

$$z_A d\overline{n_A} = z_B d\overline{n_B},\ z_A dn_A = z_B dn_B \tag{4.6}$$

The information from Eqs. (4.5) and (4.6) can be inserted into Eq. (4.4). Without additional forces, the chemical potential of the solvent in both phases is the same. Then replacing the activities from Eq. (4.2) gives the equilibrium constant: (Lito et al., 2012)

$$K_{AB} = \left(\frac{\bar{a}_A}{a_A}\right)^{z_b} \times \left(\frac{a_B}{\bar{a}_B}\right)^{z_a} \tag{4.7}$$

Where a is the activities and the top bar represents solid phase. The K_{AB} value is a true thermodynamic constant at constant temperatures as it only depends on temperature. (Dranoff and Lapidus, 1957) If nonideal behavior is suspected, the correct selectivity coefficient $K^A{}_{aB}$ takes into account the effects of involved activity coefficients γ. It is also known as apparent equilibrium constant: (Soldatov, 1995)

$$K_{aB}^{A} = K_{AB} \times \left(\frac{\gamma_B^{z_a}}{\gamma_A^{z_b}} \right) \tag{4.8}$$

4.3 Multicomponent Modeling with Binary Systems

As with the case of using ion exchange to gather lithium, nickel, cobalt and manganese from acid leachate (Kushnir, 2015), many ion exchange processes contain multiple components. One of the most common ways to approach multicomponent systems is to use data from binary systems (Provis et al., 2005). The multicomponent system is divided into consecutive binary systems, that contain the exchange of each ions included in the system (Vo and Shallcross, 2003). For example, if a system contains three cations, the multicomponent system can be divided into the following reactions: (Dranoff and Lapidus, 1957)

$$\bar{A}^+ + B^+ \rightleftharpoons \bar{B}^+ + A^+ \tag{5.1}$$

$$\bar{A}^+ + C^+ \rightleftharpoons \bar{C}^+ + A^+ \tag{5.2}$$

$$\bar{B}^+ + C^+ \rightleftharpoons \bar{C}^+ + B^+ \tag{5.3}$$

where the top bar represents the solid phase. The equilibrium constants for the ionic species is thought to be independent of any other ionic species (Vo and Shallcross, 2003). This is usually done to simplify the high amounts of complexity inside multicomponent systems. Heterogeneity of the resin's surface, effects of competitive ions, interactions with counterions and clustering of ions cause complex non-idealities in the system. (Lito et al., 2012)

4.3.1 Ideal Model

If the activity coefficients are presumed to be 1 for all of the ions, the selectivity constant presented in eq. (5) can be explained with concentrations as follows: (Dranoff and Lapidus, 1957)

$$K_c = \left(\frac{[\bar{A}^+]^{z_b}[B^+]^{z_a}}{[A^+]^{z_b}[\bar{B}^+]^{z_a}}\right) \tag{6}$$

where the brackets represent concentrations and top bar represents the solid phase. With this knowledge, the equilibrium constants for each binary reaction showcase in equations (5.1), (5.2) and (5.3) can be calculated. It should be noted that the equilibrium gained from using eq. (6) is not a true thermodynamic constant, since it now depends on the concentrations in both the resin and solution. (Lito et al., 2012)

4.4 Activity Coefficient Models

The problem with assuming both ion exchange phases to be ideal, is that these models proved to be inaccurate, because of the nonideal behavior in both phases. (Vo and Shallcross, 2005) These nonideal behaviors are crucial even in low concentrations, because of the ions interacting strongly in the system due to their electric charges (Lito et al., 2012). In order to achieve an accurate model of ion exchange using the mass action law approach, the activity coefficients, that are thought to be 1 in ideal situations, need to be accurately derived for both the solution and resin phases. (Aniceto et al., 2012) Multiple models have been developed to predict the equilibrium behavior of ion exchange processes (Vo and Shallcross, 2005). The models can be divided into solution phase and exchanger phase models, depending on, which phase is being modelled. (Lito et al., 2012)

4.4.1 Debye-Hückel Model

Debye-Hückel model takes the ionic strength I into consideration when determining the activity coefficient. The limiting law is as follows: (Aniceto et al., 2012)

$$Ln\,\gamma = -\frac{A_\gamma z_i^2\sqrt{I}}{1+\beta_{DH}a_{min}\sqrt{I}} \tag{7.1}$$

With

$$I = \frac{1}{2}\sum_{i=1}^{n} z_i^2 m_1 \tag{7.2}$$

$$A_\gamma = \left(\frac{e^2}{\varepsilon k_B T}\right)^{3/2}\sqrt{\frac{2\pi\rho_w N_0}{1000}} \tag{7.3}$$

$$\beta_{DH} = \sqrt{\frac{8\pi e^2 N_0 \rho_w}{1000\varepsilon k_B T}} \tag{7.4}$$

where A_γ is the Debye-Hückel constant, N_0 represents Avogadro's constant, a_{min} is an approximated minimum distance between ions, ρ_w is density, T is temperature, e is electron charge, ε is dielectric constant n is the number of ionic species, m is molality and k_B represents Boltzmann's constant.

4.4.2 Pitzer Model

Debye-Hückel model is applicable in very dilute solutions. This is due to the dominance of long-range interactions in the system. (Laatikainen, 2011) In higher concentrations, the effects of short-range interactions become unavoidable. The Debye-Hückel model ignores these effects, making it applicable up to 0.1 molal ionic strengths. (Pitzer, 1973) This is why other models for determining activity coefficients in the solution need to be applied, especially in the case of LIBs, where the concentration of the metal ions in the leachate can be quite high.

The Pitzer model introduces an idea that the short-range forces between ions also depends on ionic strength. Including a second virial coefficient, that is dependent on ionic strength increases the accuracy of the model at much higher concentrations. When the ionic strength in a system increases, the second coefficient decreases. (Pitzer, 1973) The Pitzer model is therefore, an extension of the Debye-Hückel model that takes the short-range binary and ternary interactions into account (Kim and Frederick, 1988). The Pitzer model equations for determining the activity coefficients for cations *c* and anions *a* are as follows: (Pitzer, 1991)

$$Ln\,\gamma_c = z_c^2 F_{DH} + \sum_j m_j \left\{ 2B_{cj} + \left(2\sum_i m_i z_i \right) c_{cj} \right\} + \sum_i m_i \left(2\Theta_{ci} + \sum_j m_j \Psi_{cij} \right) + \sum_i \sum_j m_i m_j \left(z_c^2 B'_{ij} + |z_c| c_{ij} \right) + \frac{1}{2} \sum_j \sum_{j'} m_j m_{j'} \Psi_{cjj'} \tag{8.1}$$

$$Ln\,\gamma_a = z_a^2 F_{DH} + \sum_i m_i \left\{ 2B_{ai} + \left(2\sum_j m_j z_j \right) c_{ai} \right\} + \sum_j m_j \left(2\Theta_{aj} + \sum_i m_i \Psi_{aij} \right) + \sum_i \sum_j m_i m_j \left(z_a^2 B'_{ij} + |z_a| c_{ij} \right) + \frac{1}{2} \sum_i \sum_{i'} m_i m_{i'} \Psi_{aii'} \tag{8.2}$$

In equations (8.1) and (8.2) the subscripts *j* and *i* represent all cations and anions in the solution. Θ and Ψ are only present in multicomponent solutions. Θ includes interactions between two cations or two anions, and Ψ includes interactions with two cations and one anion or two anions and one cation. F_{DH} contains the contribution of the Debye-Hückel model and takes into consideration the far field interactions between ions. (Lito et al., 2012) It is showcased in equation (8.3). (Pitzer, 1991)

$$F_{DH} = -\frac{A_\gamma}{3} \left[\frac{\sqrt{I}}{1+1.2\sqrt{I}} + \frac{Ln(1+1.2\sqrt{I})}{0.6} \right] \tag{8.3}$$

The second virial coefficient *B* in eqs. (8.1) and (8.2) represent the interactions of ion pairs that have opposite charges. They are calculated as follows:

$$B_{ij} = \beta_{ij}^{(0)} + \beta_{ij}^{(1)} g\left(\alpha_1\sqrt{I}\right) + \beta_{ij}^{(2)} g\left(\alpha_2\sqrt{I}\right) \tag{8.4}$$

$$B'_{ij} = \frac{+\beta_{ij}^{(1)} g'\left(\alpha_1\sqrt{I}\right) + \beta_{ij}^{(2)} g'\left(\alpha_2\sqrt{I}\right)}{I} \tag{8.5}$$

Finally, C_{ij} is defined by Pitzer to be:

$$C_{ij} = \frac{C_{ij}^{(0)}}{2\left|z_i z_j\right|^{0.5}} \tag{8.6}$$

The values of $C_{ij}^{(0)}$, $\beta_{ij}^{(0)}$, $\beta_{ij}^{(1)}$ and $\beta_{ij}^{(2)}$ are compound dependent values found in literature. The α value is based on the salt's valency. For monovalent ions α_1 is 2 and α_2 is 0, and for higher valences the values are 1.4 for α_1 and 12 for α_2. Knowing these, it is possible to determine the variables C and B. The functions g(x) and g'(x) are as follows:

$$g(x) = \frac{2[1-(1+x)\exp(-x)]}{x^2} \tag{8.7}$$

$$g'(x) = \frac{-2\left[1-\left(1+x+0.5x^2\right)\exp(-x)\right]}{x^2} \tag{8.8}$$

Because of the high number of parameters, that can be adjusted, the Pitzer model is very useful in fitting experimental data. The Pitzer model has been proven to produce very accurate results, when calculating the activity coefficients in a solution. (Xiong, 2006) However, the availability of the entire set of the needed parameters can be somewhat scarce, especially for complex ions. Because of this, some simplifications may be necessary to get reliable results. (Wang et al., 1997)

4.4.3 Wilson Model

Whereas the Debye-Hückel and Pitzer models described non-idealities in the solution, the non-idealities occurring in the ion exchanger also need to be considered. One of the most common ones is Wilsons model. It was originally designed for obtaining vapor-liquid equilibrium. (Aniceto et al., 2012) The strength of the model is that in a binary system, only two parameters Λ_{ij} and Λ_{ji} are required to calculate the exchanger phase activity coefficient. The parameters Λ_{ij} and Λ_{ji} just

showcase a deviation from ideality, because if their value is 1, the exchanger phase is ideal. (Vo and Shallcross, 2003) For a binary system, where *j* and *i* represents cations and anions, the Wilson model simplifies into: (Aniceto et al., 2012)

$$Ln\bar{\gamma}_i = Ln\left(y_i + y_j \Lambda_{ij}\right) + y_j \left[\frac{\Lambda_{ij}}{y_i + y_j \Lambda_{ij}} + \frac{\Lambda_{ji}}{y_j + y_i \Lambda_{ji}}\right] \tag{9.1}$$

where y is the mole fractions of anions and cations. The parameters Λ_{ij} and Λ_{ji} can be calculated using molar volumes v, ideal gas constant R and characteristic energy difference λ_{ij}-λ_{ii} with the following equation: (Aniceto et al., 2012)

$$\Lambda_{ij} = \frac{v_j}{v_i} exp\left(\frac{\lambda_{ij} - \lambda_{ii}}{RT}\right) \tag{9.2}$$

After calculating the parameters for a binary system of an ion and a counter ion, the parameters for a multicomponent system can be determined. The problem with the nonideal behavior in the solid phase is the differences of ion exchange materials and the sensitivity of the Wilson model to changes in the experimental data. (Petrus and Warchoł, 2005)

4.5 Ion Adsorption

Ion exchange can be described with the law of mass action. However, the nonidealities can also be explained with the heterogeneity of functional groups in the ion exchange resin. (Melis et al., 1996) When examining the process through this statement, an adsorption isotherm is used instead of ion exchange isotherms. These adsorption isotherms are mathematical, and they address the heterogeneity of the ion exchanger with two or more parameters, that are adjustable. This makes

them very flexible over wide range of different types of experimental data. (Petrus and Warchoł, 2005)

4.5.1 Extended Langmuir Model

Langmuir model is a popular application of models that describe ion exchange as an adsorption process (Lito et al., 2012). The basic idea of the model is that the uptake of ions into the ion exchange resin only occurs on the resin's surface in active sites. The model does not in differentiate between ion exchange or adsorption. (Carmona et al., 2006) However, this basic Langmuir model is not applicable for multicomponent systems. Therefore, an extended Langmuir is used for multicomponent applications. The extended Langmuir model goes as follows: (Putro et al., 2017)

$$q_E = q_m \frac{K_{j,i} c_{E,j}}{1+\sum_{j-1}^{n} K_c c_{E,i}} \tag{10}$$

where q_m and K represent Langmuir constants while c represents the concentrations of counterions from the exchanger in the solution and solid phase. Problems arise, when using the extended Langmuir model, because it is unable to track the competition of the ions in the sorption sites. Without taking the competition into account, the extended Langmuir model overestimates the isotherm values. To counter this shortcoming, predictions are required for the adsorption equilibria for the binary components in the system. The extended Langmuir model has been generally used for binary systems. For example, the adsorption of lead and mercury from aqueous solutions have been studied using this model (Putro et al., 2017) However, it is not favorable for chemically complicated systems like LIB recycling, because of the high amount of different ions in the system.

4.5.2 Freundlich Model

Another adsorption-based model, that is used to describe adsorption or ion exchange, is the classical Freundlich model. The Freundlich model utilizes another adsorption isotherm. It differs from the one used in the Langmuir model in its key assumptions. Where the Langmuir model assumes the surface of the resin to be homogenous, the Freundlich model assumes heterogenous surface structure. Key differences also arrive in the behavior of the sorbed species. Freundlich model assumes that the interactions between sorbed species, can be possible. In the Langmuir model, these interactions are not occurring. Because of these differences, both of these models cannot be valid at the same time. (Kónya and Nagy, 2013) The classic version of the Freundlich model can be written as: (Kinniburgh et al., 1983)

$$q_E = k_f + c_E{}^{\frac{1}{n}} \tag{11}$$

where q is the concentration of metal in the solid phase, k_f represents the Freundlich constant, c is concentration of the metal in solution and $1/n$ is an empirical constant that indicates the adsorption intensity.

The Freundlich model does not account for saturation. Because of this, when the sorbate concentration increases, so does the amount of adsorbate. (Li et al., 2014) One of the big drawbacks of using this model is that it does not account for the number of binding sites in the resin. Because of this, it can only be under certain window since it cannot be used for extrapolations. Extrapolating generates exponential distribution of binding sites in the system. (Kumar et al., 2010) Because of this drawback, the Freundlich model is not applicable for process modelling.

4.6 Surface Complexation Model

Surface complexation model (SCM) focuses on the binding process, that is happening at the adsorption site. This model is particularly suitable for systems with high affinity. (Laatikainen, 2011) The basic idea of SCM is that cationic and anionic species from the solution phase form ion

pairs at the surface of the ion exchanger. These pairs are called surface complexes, and they occur because of the amphoteric surface sites that are generated by the surface charge. (Jeon and Höll, 2004) The charged are generated by either protonation or dissociation of the surface groups. The surface of the resin is considered to have a surface, where the functional groups are distributed uniformly. Because of this functionality, only protons and hydroxide ions are assumed to be adsorbed directly at actual surface of the resin. The other ions present in the system are located in Stern layers that are parallel to the surface of the resin. (Stöhr et al., 2001) This phenomenon is showcased in Figure 3.

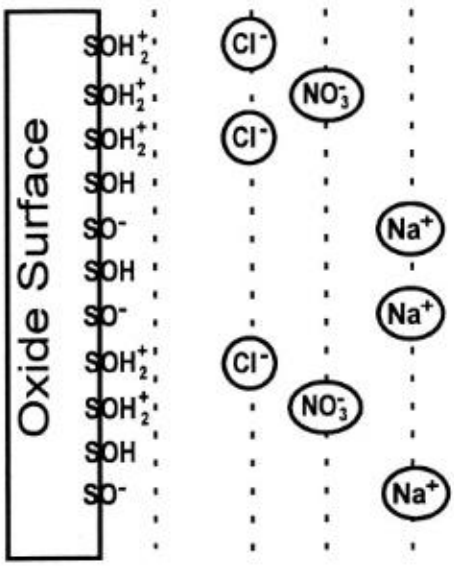

Figure 3. The arrangement of ions in a system containing Cl^-, NO_3^- and Na^+ ions. (Höll and Horst, 1997)

Figure 3 showcases that the charges on the surface are balanced via counterions in the Stern layers. Because of this, the surface potential decreases to 0 in the solution phase. The order of the ions in the layers depend on the size of the ion. Because of this, the larger anions are closer to the surface than the smaller cations. (Höll and Horst, 1997)

For SCM the electrical potentials, that are unknown, need to be eliminated. This is done by considering two Stern layers as electric capacitors. For this reason, a relationship of resin loading, and metal salt is generated. The simplified equations can be written as: (Stöhr et al., 2001)

$$logQ_{MX} = logK_{MX} + m_{SCM,2} \cdot y(X) \tag{12.1}$$

$$logQ_{H_2X} = logK_{H_2X} + m_{SCM,1} \cdot y(H) + m_{SCM2} \cdot y(X) \tag{12.2}$$

where *K* is the equilibrium constant, *y(X)* represents the dimensionless loading of anions, *Q* is separation factor. The subscripts of the equilibrium constants represent the acid H_2X and the metal salt *MX*. The terms m_1 and m_2 can be determined with:

$$m_{SCM,1} = -\frac{B_{SCM}}{C_1(H,M)} \tag{12.3}$$

$$m_{SCM,2} = -\frac{B_{SCM}}{C_2(H,M)} \tag{12.4}$$

$$B_{SCM} = \frac{2 \cdot F^2 \cdot q_{max}}{\ln 10 \cdot R \cdot T \cdot A} \tag{12.5}$$

where *A* is surface area, *F* is Faraday's constant and *C* is the electric capacitance (F/m^2) formed by the protonated surface and the first layer of metal ions. These equations make describing the equilibrium feasible, since only parameters *m* and *K* are required. These parameters can be easily obtained by using experimental data. When Q_{MX} is plotted as a function of dimensionless loading with anions y(X), the intersection of the plot gives the parameter log K_{MX} and the slope is the parameter m_1. For K_{H2X}, log Q_{MX}-m_2y(X) is plotted as a function of y(H), which is the loading of protons. These are all for binary systems. However, adding more components just adds new parameters *K* and *m*, but the numerical values of *K* and *m* from the binary systems stay the same. (Stöhr et al., 2001) The relationships between parameters in binary and ternary systems can be written as: (Jeon and Höll, 2004)

$$lnK_{binary} = lnK_{ternary} \tag{12.6}$$

$$m_{SCM,1_{binary}} = m_{SCM,1_{ternary}} \tag{12.7}$$

$$m_{SCM,2_{binary}} = m_{SCM,2_{ternary}} \tag{12.8}$$

SCM has been utilized in various system. A common application is modeling heavy metal adsorption sorption with different types of resins. Sorption processes containing copper, nickel and cadmium have been accurately modeled with SCM. SCM can accurately predict the dimensionless loadings of these metal ions in the liquid phase as is seen in Figure 4. (Jeon and Höll, 2004) (Stöhr et al., 2001)

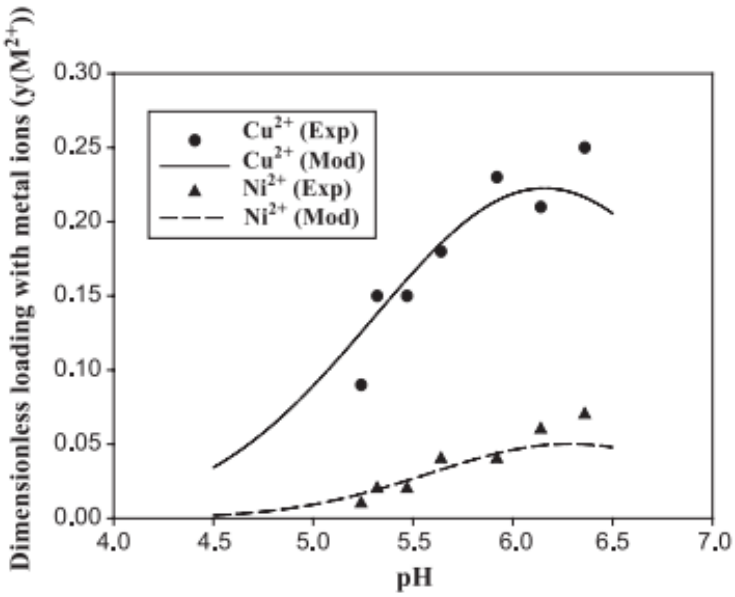

Figure 4. Experimental and modelled dimensionless loading copper and nickel ions in the liquid phase. (Jeon and Höll, 2004)

It should be noted, that because of the reliance of the assumption, that the functional groups are distributed on a plane surface, the model is applicable for rigid macroporous resins. If the ion exchange resin is not a cross-linked and weakly acidic or basic, the model cannot anticipate the behavior of a system. For gel type resins, the SCM produces false ion profiles because of the gel type resin and solution exist entirely in separate phases. (Marinsky, 1996)

4.7 Non-ideal Competitive Adsorption

Understanding the interactions between metal ions and organic matter has been an important factor, because of the impact that different metals can have in different industries, groundwaters and surface waters. The challenge of formulating such models, is the complexity of the system due to the heterogeneity present in the organic matter. (Kinniburgh et al., 1999) In order to understand a multicomponent system, three general steps need to be considered. The first one is competition. Every cation in the system competes for the same sites on the ion exchange resin. This influences the binding equations. The second thing to consider is the affinity distribution of individual ions. The final thing to consider, is the stoichiometry of the reactions occurring in the system. Without this consideration, the amount of metal ions that can be bound, would be the same for protons as well. However, multivalent cations have different stoichiometry with the binding sites than the proton. (Koopal et al., 2005) This idea mimics the basic principle of the Freundlich isotherm presented in part 4.5.2. The Freundlich isotherm considers the interactions between species in the process. These interactions are vital when dealing with multicomponent systems.

Non-ideal competitive adsorption (NICA) is a model that tries to describe the phenomena present in a multicomponent system. Because of the complexity of a system, where each individual ion's affinity is considered, NICA makes assumptions to make simplifications. The main assumption is that there is perfect correlation between the individual affinity distributions. This assumption makes it so that only one parameter is required for each metal ion to make the model competitive ion binding. (Koopal et al., 2005) NICA also assumes a continuous distribution of affinities. The significance of NICA compared to previous models is that it accounts for different median affinities for each ion, but it also includes ion specific nonidealities and heterogeneity. (Kinniburgh et al., 1996) The NICA isotherm can be written as: (Sirola et al., 2008)

$$q_i = q^{max} \sum_{k=1}^{L} \omega_k \left(\frac{h_{1,k}}{h_{H,k}}\right) \frac{(\kappa_{i,k} c_i)^{h_{i,k}} \left[\sum_j (\kappa_{j,k} c_j)^{h_{j,k}}\right]^{p_k^{-1}}}{1+\left[\sum_j (\kappa_{j,k} c_j)^{h_{j,k}}\right]^{p_k}} \tag{13.1}$$

where q is amount bound in the solid, q^{max} is the total amount of sorption sites, k describes the heterogeneity of a sorption site, ω is the fraction of k-type sites in the system, and c is the solution concentration. The subscripts i and j represent the components, h is a parameter depending on the

binding stoichiometry. L describes the amount different types of sites. and p_k represents the width of the site strength distribution and it characterizes the heterogeneity of the site. The value of κ is the affinity constant and it can be obtained from the following equation: (Laatikainen, 2011)

$$ln\kappa_i = ln\kappa_i(T_0) + \frac{\Delta H_{ads}}{R}\left(\frac{1}{T_0} - \frac{1}{T}\right) \tag{13.2}$$

where ΔH_{ads} is the adsorption enthalpy, T represents temperature and R is the ideal gas constant.

There are decisions that must be made when fitting experimental data to NICA-type models. It is important to decide how the data is used. Whether to fit all data simultaneously or in different batches. Small datasets may cause problems and some restrictions on the parameters might be necessary. Because the combination of different types of data is crucial, the uncertainties in the data, need to be considered. (Kinniburgh et al., 1999) However, NICA has been used successfully when modelling breakthrough curves for multicomponent systems. Especially, when metals such as nickel and copper need to be removed from zinc rich solutions, NICA has been utilized various times for predicting the movement of ions in the system. This can be seen in Figure 5. (Laatikainen and Laatikainen, 2016)

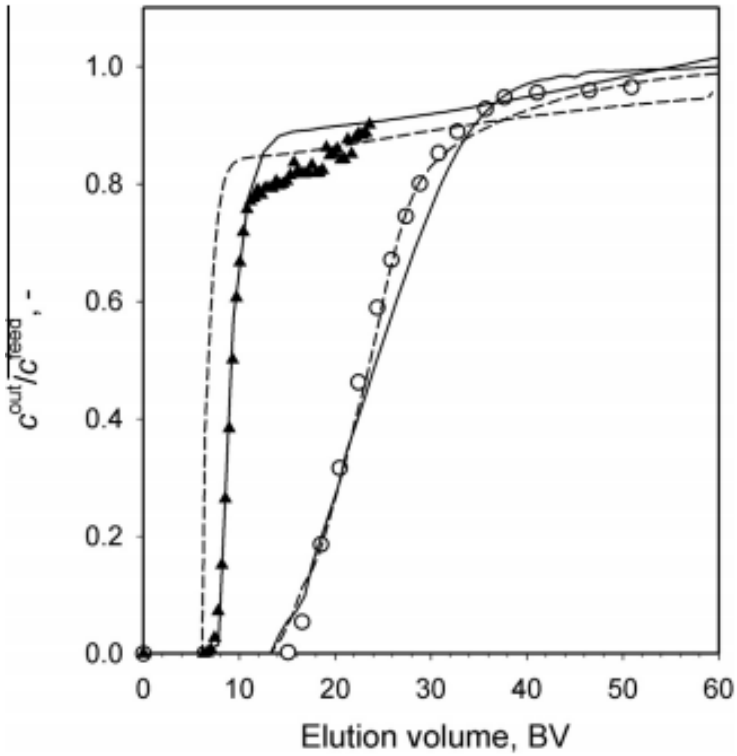

Figure 5. Breakthrough curves for nickel and zinc. Nickel is represented with circles while zinc is pictured with triangles. Temperature in the column was 25 ˚C, feed flow was 11 BV/h and zinc concentration were 0.00965 mol/L. CuWRAM was selected as the resin. Dashed lines were calculated using NICA and solid lines were calculated with a chelating model. (Laatikainen and Laatikainen, 2016)

It should be noted that in systems, where bidentate structures are present, NICA has a weakness. Because NICA assumes the maximum ion exchange ratio to be one because of monodentate binding, a presence of bidentate structures can cause the exchange ratio to fluctuate between 1-2. This is especially the case with copper, that can form bidentate chelate-type structures. This type of binding is not accounted for in the NICA model. (van Riemsduk et al., 1996)

5. Kinetics of Ion Exchange Processes

The ion exchange kinetics represent the speed of the reactions taking place inside the system. The rate of the exchange needs to be considered, when designing an ion exchange process. Mass transfer resistance in the solution and solid phase plays a large part in the kinetics of the system. Other affecting factors are concentrations, temperature and the type of resin used. (Nasef and Ujang, 2012) There are six steps, that take place in an ion exchange process. Any one of them, or combination of them, can be the rate controlling step of the process. The steps are: The ion exchange reaction, diffusion of counter ions through either the bulk solution or a hydrated film, diffusion of counter ions within the resin and diffusion of exchange species either out of the ion exchange resin or from the resin surface to the solution. Because the ion exchange reaction happens very rapidly, it is not considered to be the rate limiting step of the process. The rate limiting step is then either particle diffusion or film diffusion. The slower of these steps is considered to control the overall reaction rate. However, In intermediate cases, both steps can affect the overall rate. (Helfferich, 1995)

5.1 Mass Transfer

Mass transfer inside the solid particles happen because of diffusion. The rate of the diffusion depends on the structure of the resin, properties of the species and interactions occurring between the functional groups of the ion exchanger and the migrating species. Simplifications are usually applied with the external mass transfer in the liquid film, that surrounds the solid particles. The physical properties of the diffusing species affect the mass transport parameters. However, their inclusion into the formulation of a model is not necessary. With the case of ions, the electrostatic contribution needs to be considered. (Laatikainen, 2011)

The models used to describe the mass transfer in the solid phase are divided into three groups based on their approach to the modelling of the mass transfer. The exact models utilize the formulation of inter particle concentrations. This is the most used approach in a theoretical environment. However, the use of these exact models in simulations can be quite difficult in a multicomponent system, because the complexity of computing such a model. In order to solve this arising

complexity problem, solutions that apply some approximations are utilized. The final group of models consists of empirical end semiempirical models that have similarities with reaction kinetics of ion exchange. However, this final group of models are not applicable in multicomponent systems with different types of equilibrium conditions. (Laatikainen, 2011) Therefore they are not included in this thesis, because of their low value regarding the kinetics of ion exchange of LIB leachate.

5.2 Fick's Law

Fick's law describes the flux of ions through a solid phase. When the solid phase comes in to contact with a solution containing ions, diffusion process takes place. Fick's law-based models are generally described as homogenous diffusion models, since it assumes that the solid particle has a homogenous structure. (Lito et al., 2012) If electrochemical gradients are ignored, the first Fick's law can be used to describe the flux *J* with the following equation. (Chowdiah and Foutch, 2002)

$$J_i = -D_i \frac{\partial q_i}{\partial r} \tag{14.1}$$

where *D* is the diffusion coefficient, *r* represents the radial coordinate and *q* is the concentration in the solid phase. Fick's law is applicable for systems, that have constant diffusion coefficients. The flux *J* can be utilized when it is combined with the material balance of a sphere. (Chowdiah and Foutch, 2002)

$$\frac{\partial q}{qt} = D\left(\frac{\partial^2 q}{\partial r^2} + \frac{2}{r}\frac{\partial q}{\partial r}\right) \tag{14.2}$$

With this equation, the evolution of the solid phase concentration and be modelled for spherical solid phase beads.

5.2.1 Nernst-Planck Model

The electric field generated by the mobilities of counter ions in the ion exchange process, introduce additional forces into the system. This force transferences the ions in the system. Compared to classical models based on the Fick's law, the Nernst-Planck model accounts the influence of the generated electric force. In the Nernst-Planck model the transference of a species in the current's direction is proportional to the concentration, valence and electric potential. (Lito et al., 2012) The molar ion flux *N* occurring in the resin can be written with the following equation: (Costa et al., 2010)

$$N = D_i \left[\frac{\partial q_i}{\partial s} + z_i q_i \frac{F}{RT} \frac{\partial V}{\partial s} \right] \tag{15}$$

where *s* represents the distance to symmetry plane, *q* is the concentration in the resin, *V* represents the electric potential, *D* is the diffusivity, *z* is ion charge, *R* is ideal gas constant, *T* is temperature and *F* represents the Faraday constant.

The Nernst-Planck model was proposed as far as 1890, and it is still in wide use amongst authors. However, using this model is quite problematic. The diffusion equations do not consider law of mass to the total solution. The model also does not account the balance equation of the momentum. (Dreyer et al., 2013)

5.2.2 Stefan-Maxwell Model

Stefan-Maxwell model is the most exact for intra-particle mass transport modelling. The chemical potential gradient is utilized as a driving force in this model. The diffusion fluxes occurring in the system are completely account for in the Stefan-Maxwell model. It can also account for swelling, electrostatic interactions and hindrances on diffusion rate. (Laatikainen, 2011) The Stefan-Maxwell equations were initially designed to describe diffusion in ideal gases. However, it has been extended to cover multicomponent diffusion in solids and liquids as well. (Lin et al., 2016) The general equation can be written as follows: (Krishna and Wesselingh, 1997)

$$\frac{y_i}{RT}\nabla\mu_i = \sum_{\substack{j=1\\ j\neq 1}}^{n} \frac{1}{c_t}\frac{y_i N_j - y_j N_i}{D_{ij}} \qquad \text{I} = 1, 2, \ldots \text{n-1} \qquad (16.1)$$

where μ is the chemical potential, y represents mole fraction and N is the mole flux, c is the total concentration of the solution and D is the mutual diffusion coefficient between i and j.

Using these exact models can form very complex systems with partial differential equations. For example, the mass balance equation for a macroporous particle can be written as: (Laatikainen, 2011)

$$\varepsilon_p \frac{\partial c_{p,i}}{\partial t} + (1+\varepsilon_p)\rho_s \frac{\partial q_j}{\partial t} = \varepsilon_p \frac{\partial c_{p,i}}{\partial t} + (1+\varepsilon_p)\rho_s \sum_{j=1}^{n}\left(\frac{\partial q_i}{\partial c_{p,j}}\frac{\partial c_{p,j}}{\partial t}\right) = \frac{\varepsilon_p}{\rho_s r^2}\frac{\partial}{\partial r}\left[r^2(-J_{s,i})\right]$$

with

$$r = 0: \frac{\partial c_{p,i}}{\partial r} = 0$$

$$r = R_s: \frac{\partial c_{p,i}}{\partial r} = \frac{6\varepsilon_p}{2R_s} J_{f,i}$$

$$J_{f,i} = k_{f,i}(c_i - c_{p,i}^*) \qquad (16.2)$$

where J is the diffusion flux c and c^* are the concentrations in bulk and solid liquid interface, k is mass transport coefficient, ε is particle porosity, R_s is radius and r represents the radial coordinate of spherical symmetry.

These kinds of systems can be difficult to compute. Therefore, some general assumptions and generalizations may be necessary to provide models a good compromise between accuracy and simplicity. (Lito et al., 2012) In cases, where the concentrations of ions are low or some selected compounds have much faster reaction rates, the approximate calculations can be utilized instead of exact models. (Plazinski, 2013)

5.2.3 Linear Driving Force

The basic idea of a model, like the Linear Driving Force LDF, is to simplify the system. This is done by relating the uptake rate to the average concentrations in the resin instead of concentration profiles. (Laatikainen, 2011) According to LDF the material balance can be written as: (Lito et al., 2012)

$$\frac{d}{dt}\left(\varepsilon_p c_{p,i} + q_i\right) = k_{LDF,i}(q_i^* - q_i) \tag{17.1}$$

$$\frac{1}{K_{LDF,i}} = \frac{R_S^2}{15D_{eff,i}} + \frac{1}{k_f A_{ext}} \tag{17.2}$$

where A_{ext} is the external surface area and q^* is the equilibrium concentration of the resin.

The LDF system valid only for linear isotherms. It fails in systems, where electrolyte adsorption is highly favorable and nearly irreversible. LDF can only give reasonable accurate results in moderately favorable systems. (Laatikainen, 2011) To combat the low correlation with LDF, it can be combined with other models to obtain better results. One of these models, that showcase potential, the shrinking core model. The LDF value of k can be attained with the following equations: (Sirola et al., 2008)

$$k_{p,i} = \frac{10D_{p,i}}{d_s} \tag{17.3}$$

$$k_{p,i} = \frac{2D_{p,i}}{d_s}\left[1 - \left(1 - \frac{\bar{q}_i}{q_i^*}\right)^{1/3}\right]^{-1} \tag{17.4}$$

In this model, the steady state number of adsorbed electrolytes in the solid phase q^* is larger than the average $\bar{q}$. The model in (17.4) is used until the value of k from (17.3) is obtained.

5.3 Column Dynamics

Establishing an effective ion exchange process requires, in addition to equilibrium and kinetics, the understanding of the column dynamics. The column dynamics are presented via differential mass balances for both phases. The column dynamic models can be divided into heterogenous and homogenous. Heterogenous models consider both phases, while homogenous models are one-phase models. For column dynamics, the same difficulties, when developing a model, are present. Accounting for each different phenomena occurring in the system has proven to be quite difficult. (Warchoł and Petrus, 2006) Knowing the column dynamics helps designing industrial scale processes from experimental data, that is gained from laboratory scale experiments. (Borba et al., 2011) The fixed bed column mass balances in the liquid phase can be written as: (Borba et al., 2011)

$$\frac{\partial c_i}{\partial t} + \frac{\rho}{\varepsilon}\frac{\partial q_i}{\partial t} = D_L \frac{\partial^2 c_i}{\partial z_c^2} + u\frac{\partial c_i}{\partial z_c} \tag{18}$$

where D_L is axial dispersion coefficient, z_c is axial coordinate, ε is porosity, q is the concentration of species i in the solid phase, ρ is density and u is interstitial velocity.

5.3.1 General Rate Model

The most comprehensive heterogenous model is the General Rate Model (GRM). GRM accounts for several of the most important factors in the column. These factors include external mass transfer resistance, pore diffusion, axial dispersion and film diffusion. For this reason, GRM includes two different mass balance equations. One of the equations is for the solid particles and the other is for the column. These equations can be written as: (Qamar et al., 2014)

$$\frac{\partial c}{\partial t} + u\frac{\partial c}{\partial z_c} = D_L \frac{\partial^2 c}{\partial z_c^2} - \frac{3}{R_s}\frac{1-\varepsilon}{\varepsilon} k_{ext}(c - c_p(r = R_s) \tag{19.1}$$

where t represents time, c and c_p represent the concentrations in the solution and particles, ε is external porosity, k_{ext} represents the external mass transfer coefficient, R_s represents the particle radius and r is the radial coordinate. The equation shown in Eq. (19.1) represents the mass balance of single component going through the column, that is filled with particles. The second mass balance equation, that accounts for the intraparticle diffusion in the stationary phase can be written as: (Qamar et al., 2014)

$$\varepsilon_p \frac{\partial c_p}{\partial t} + \left(1 + \varepsilon_p\right) \frac{\partial q}{\partial t} = \frac{1\partial}{r^2 \partial r}\left(r^2 \left[\varepsilon_p D_p \frac{\partial c_p}{\partial r} + (1 - \varepsilon_p) D_s \frac{\partial q}{\partial r}\right]\right) \tag{19.2}$$

where q is the amount of species in the resin phase, D_s is the surface diffusivity, D_p is the pore diffusivity and ε_p represents the internal porosity. For regenerated column, the initial conditions in Eq. (18.1) and Eq. (18.2) are c(0,z)=0, q(0,z,r)=0 and c_p(0,z,r)=0.

6. Ion Exchange Column Operation

Conventionally ion exchange processes have been batch or column operations. Common feature of the process in both batch and column operations is the cyclic nature of the process. Every ion exchange process can be divided into three separate steps. These are sorption, elution and regeneration. In sorption, the metals in the solution pass through a vessel where the desired ions attach to the resin bed while the same charge ions in the resin initially are released. In the elution stage, the ions attached to the resin are released with a solution called eluent. This eluent releases the desired ions from the vessel. Elution is sometimes referenced as stripping. Regeneration is usually done with an acid with excess of protons or alkali with hydroxide ions. The purpose of this step is to replace the ions in the resin with a less selective ion. The basic ion exchange process cycle is represented in Figure 6.(Nasef and Ujang, 2012)

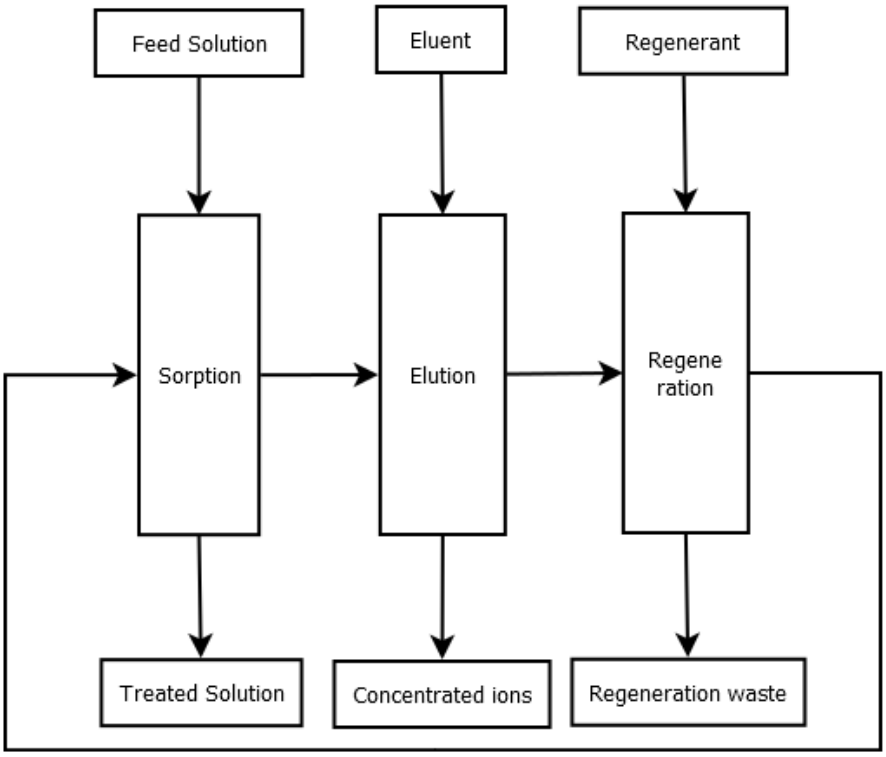

Figure 6. Basic representation of the different steps of an ion exchange process cycle. (Nasef and Ujang, 2012)

The cyclic nature of the ion exchange operation makes batch processes very tempting. However, continuous simulated moving bed (SMB) processes have seen success in different types of industries. It has clear advantages, when compared to the traditional batch operations. These include lower consumption of eluent, decreased amount of waste and more concentrated product solutions. There are two types of SMB processes. Cross-current SMB process is utilized more in industrial applications. Counter-current SMB is the other type of process that can be used for metal solution purification. SMB configurations for both cross-current and counter-current processes are showcased in Figure 7. (Virolainen et al., 2014)

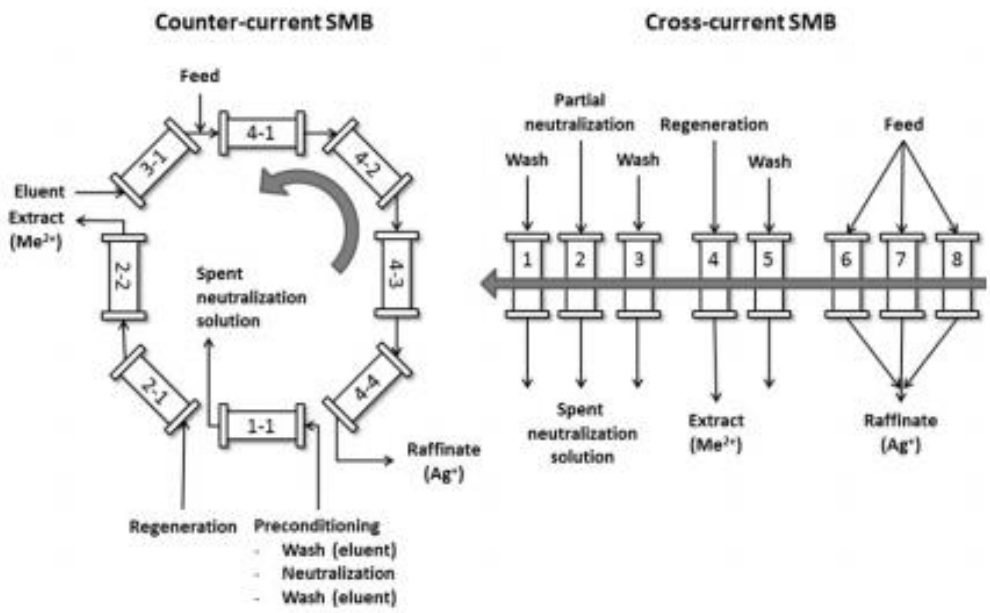

Figure 7. Cross-current and counter-current SMB operations for solution purification containing silver. (Virolainen et al., 2014)

6.1 Exchange Capacity

The capacity of the ion exchanger is an important parameter. It accounts for the number of counter ions that a specific ion exchanger can adsorb. There are several uses for the data that ion exchange capacity can be used for. The main uses are in the predesign calculations of the ion exchange

process and the knowledge of total exchange capacity of the materials. The value of capacity is often described in milliequivalents per gram or per milliliter (meq/g & meq/mL). When calculating the exchange capacity of the ion exchange resin in a packed bed or a column, distribution coefficient *K* is used. The resulting capacity is the maximum capacity of the ion exchange resin in terms of mass. The total capacity can be calculated with: (Nasef and Ujang, 2012)

$$V_{tot} = K_{AB} \times m \tag{20}$$

The use of total exchange capacity depends largely on the conditions of the process. The level of ionization and of the functional groups also plays a key role. (Nasef and Ujang, 2012)

6.2 Column Breakthrough Capacity

The breakthrough capacity is generally utilized in column-based ion exchange operations. Breakthrough capacity represents the amount of solution that can be treated before the removal of desired ionic species drastically decreases. (Nasef and Ujang, 2012) The breakthrough curve is one of the most important indicators in industrial ion exchange processes (Li and Dong, 2004). A schematic of a typical ion exchange column and a breakthrough cure are showcased in Figure 8. (Li and Dong, 2004).

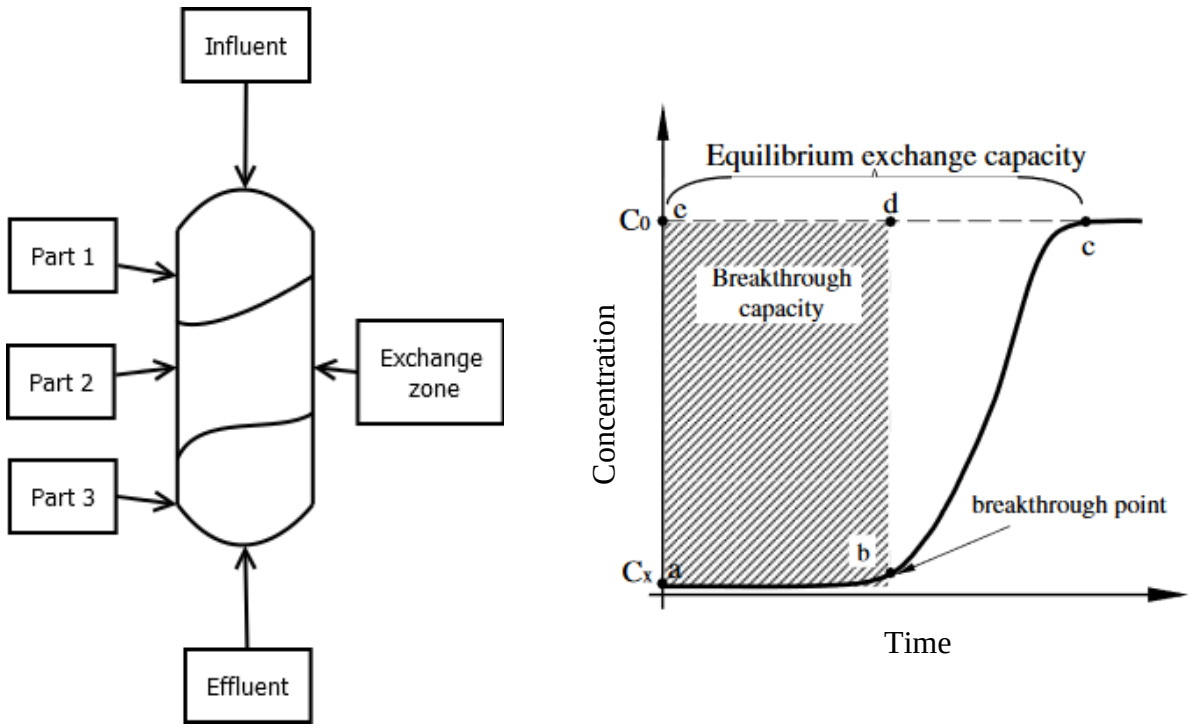

Figure 8. A typical schematic of an ion exchange column and a breakthrough curve of the process. C_0 represents the concentration in the influent and C_x represents the concentration in the effluent. (Li and Dong, 2004)

Evaluating the time, it takes the ion exchange process to reach the breakthrough point, is the focus, when sizing the bed size of the column. It is important to reach a conclusion on the time it takes for the operation to stop. In addition to just understanding the optimal process operating time, the breakthrough capacity can showcase the competitive nature of the ions, when dealing with multicomponent processes. In some cases, the outlet concentration can become higher than the inlet concentrations. This is due to the ions pushing each other out of the resin. (Inglezakis and Zorpas, 2012)

6.3 Multicomponent Metal Recovery

The presence of multiple metal ions in the system affects the overall sorption due to the competition for sites in the resin. Because of this competitive aspect in the process, the uptake of ions can be lower than with solutions containing only one component. (Lopes et al., 2012)

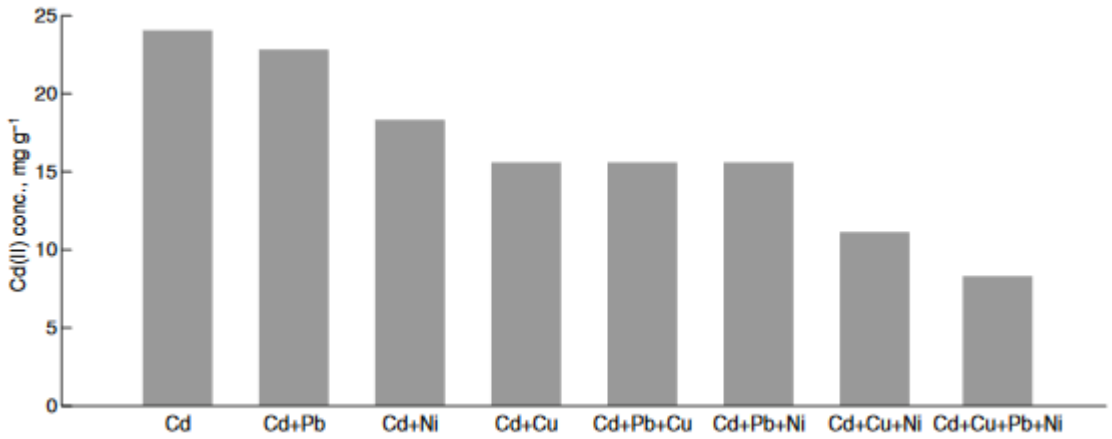

Figure 9. Cadmium uptakes for different solutions used in a cadmium sorption process. (Lopes et al., 2012)

6.4 Experimental Results for Preliminary Ion Exchange Process in LIB Recycling

The basis of the LIB recycling ion exchange process studied in this thesis, was laboratory experiments conducted earlier at LUT University in the Department of Separation Science in School of Engineering Sciences. The Experiments were done using a 4-step process cycle. The contents of the LIB leachate were based on the research of Porvali et. al. Washing was done by using deionized water and eluent was 2 M sulfuric acid. The experimental setup is showcased in Figure 10. (Kaukinen, 2019)

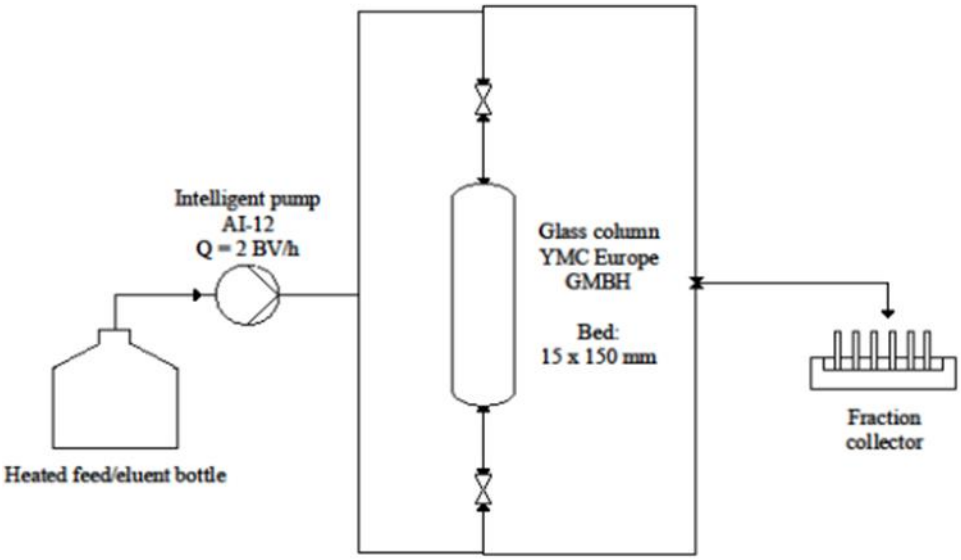

Figure 10. Experimental setup of the laboratory experiments.

While the conducted experiments were done with multiple resins, only the most promising resin Lewatit-TP-260 was selected for the modelling part of this thesis. The loading and elution data of these experiments were utilized. They can be seen in Figure 11 and Figure 12.

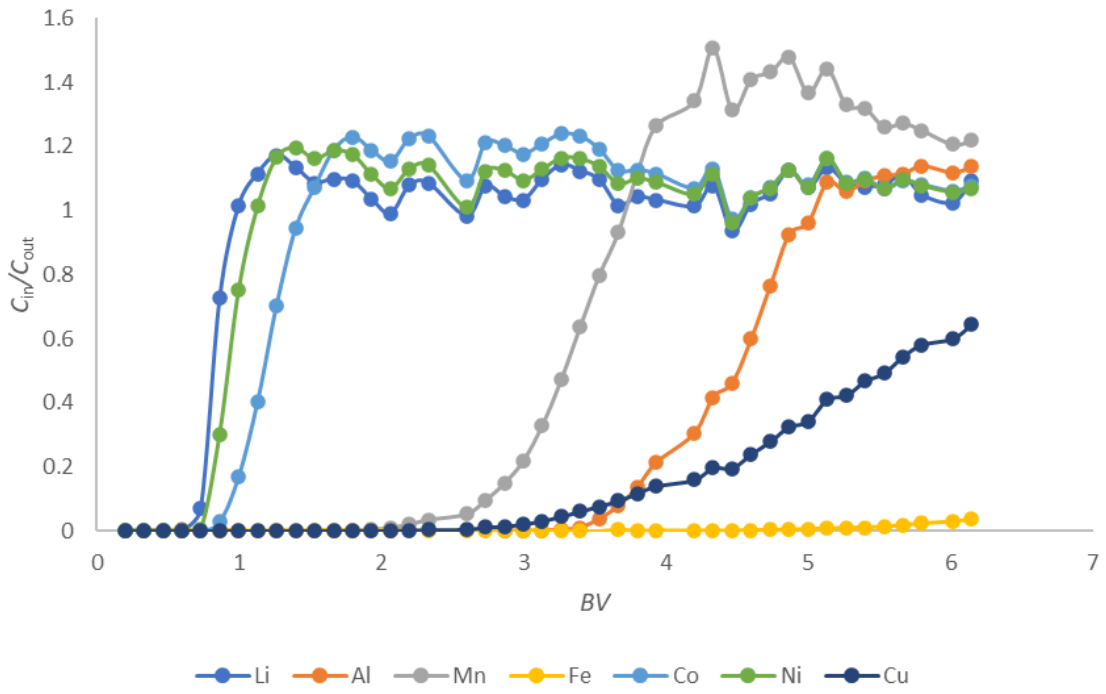

Figure 11. Laboratory experiment loading breakthrough curve for lithium ion battery leachate with LP-260. Temperature was 60 ˚C and pH was 1.8. (Kaukinen, 2019)

Figure 11 showcases how manganese breaks through at around 2.5 BV. Aluminum and copper break through at around 3.5 BV. Iron latches on to the resin very aggressively even after 6 BV. Because manganese is pushed out of the resin by the other compounds, its concentration rises above the feed solution.

After loading the reactor, the resin bed needs to be eluted. A suitable elution solution can remove most of the metals attached to the resin relatively fast. For these simulations, a 2M sulfuric acid was selected to be used in the elution just like in the experiments conducted by Kaukinen. The results can be seen in Figure 12. (Kaukinen, 2019)

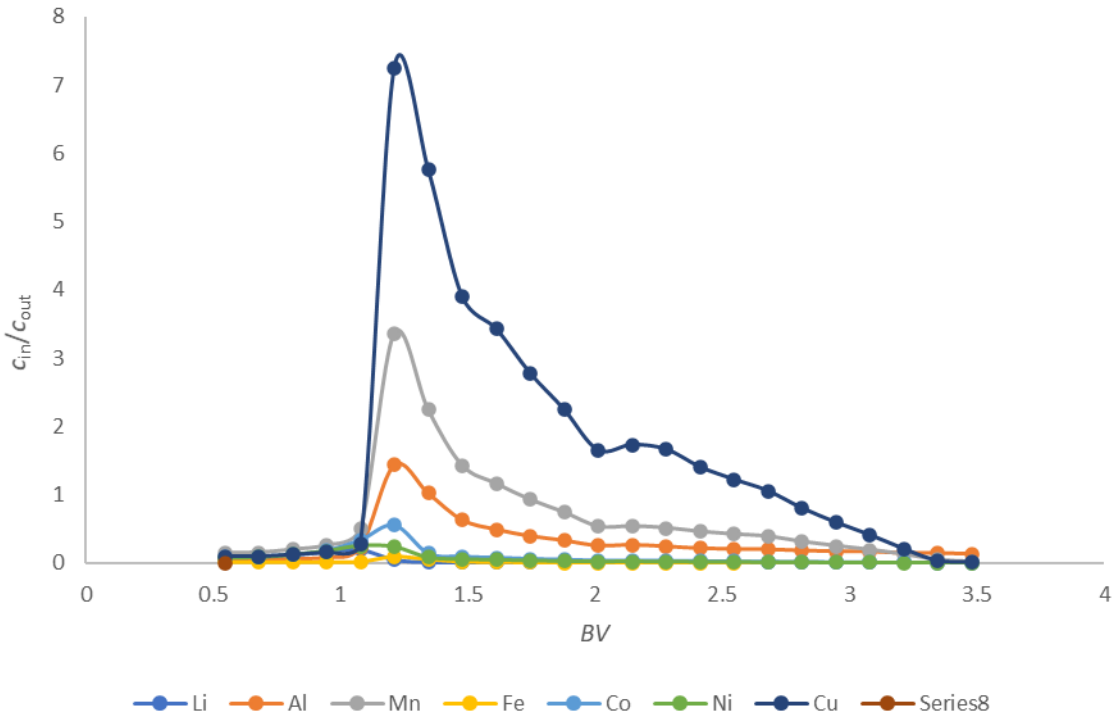

Figure 12. Elution results from laboratory experiments. Temperature was 60 ˚C and pH was 1.8. 2M sulfuric acid was used as eluent. (Kaukinen, 2019)

From Figure 12 it can be seen that copper is eluted rapidly after 1 BV. Sulfuric acid manages to remove manganese from the resin. The problems arise with aluminum because sulfuric acid fails to remove the aluminum in the resin. Potassium oxalate was suggested for aluminum and iron removal. (Kaukinen, 2019)

7 Process Simulations

The simulations of this thesis were done by using ResMod Toolbox for Parameter Estimation and Process Simulation in Ion Exchange and Adsorption by Markku Laatikainen. ResMod is used for selecting the models that are used in the calculations and the materials in the system. ResSim is used for simulating dynamic ion exchange processes for a fixed bed reactor. The overall mass balances for fixed-bed systems are considered with the following equation in this toolbox. (Laatikainen, 2014)

$$\frac{\partial c}{\partial t} + v\frac{\partial c}{\partial x} + \left(\frac{1-\varepsilon}{\varepsilon}\right)\frac{6k_f}{d_s}(c - c^*) - D_x\frac{\partial^2 c}{\partial x^2} = 0 \tag{21}$$

where ε is constant.

7.1 Ion Exchange Model

For the Lithium ion battery leachate simulations NICA-IX model was the selected ion exchange model from the ResMod tool. NICA-IX model applies well into a multicomponent system with many competing ions. NICA-IX dictates that every site in the resin must be occupied to maintain electro neutrality. Because of this electroneutrality, the equation (13.1) can be written as follows.

$$q_i = \frac{h_i}{h_{ref}}\frac{q_{max}K_i' c_i^h}{\sum_{j=1}^{N} K_j' c_j^h} \tag{22}$$

Where *ref* represents the reference ion (H^+) in the system. Macroporous Nernst-Planck equations were used for the intra-particle diffusion model.

ResMod also requires information about the components that appear in the system as well as the properties of the ion exchange resin. The properties of the resin can be seen in Figure 13.

Figure 13. The resin properties for a chelating Lewatit-TP-260 resin in ResMod. ("Lewatit-TP-260-L.pdf," 2020)

Lewatit-TP-260 was selected as the preferred resin based on initial laboratory experiments that showcased promising results, when treating lithium ion battery leachate (Kaukinen, 2019). TP-260 is a chelating weakly acidic cation exchanger. The chelating group is an amino methyl phosphonic acid group. From Figure 13 it can be seen that proton acts as a counter ion and all the sites in the resin are considered active in this case. TP-260 has a density of 720 g/L and it is a microporous resin. The charge of the site is -2 for chelating resins in ResMod.

7.2 Simulation Parameters

Every major parameter and property of the ion exchange system are given in ResSim. These include simulation parameters, properties of the fixed-bed column, properties feed of solutions, ion exchange system configuration, concentrations of metals, number of columns in the system, NICA parameters, diffusion parameter and the events of the process.

The NICA-IX and diffusion parameter were fitted visually based on the laboratory results presented in (Kaukinen, 2019). This kind of approach has seen success in previous applications in the removal of copper from an aqueous solution. However, it only 2 different components compared to the high amount of metals in lithium ion battery leachate. (Holopainen, 2016) The focus was to obtain parameters that resemble the laboratory experiments as closely as possible. The phase equilibrium and mass transfer parameters can be seen in Figure 14.

Phase equilibrium and mass transfer parameters

Component	log*K*	*h*	*Ds*, m^2/s	*Dp*, m^2/s	k_f, m/s
H	0	1	0.00E+00	1.00E-09	0.00E+00
Li	-0.8	1	0.00E+00	4.00E-10	0.00E+00
Co	-0.6	0.7	0.00E+00	4.00E-10	0.00E+00
Ni	-0.3	1.3	0.00E+00	4.00E-10	0.00E+00
Mn	-0.09	0.9	0.00E+00	8.00E-10	0.00E+00
Cu	0.3	1	0.00E+00	4.00E-10	0.00E+00
Al	0.05	0.8	0	4E-10	0
Fe	1.6	1	0	4E-10	0
SO4	-10	1	0	4E-10	0

Get equil. parameters

Save equil. parameters

Figure 14. Visually applied NICA-IX- and diffusion parameters for each component in the ion exchange system.

In Figure 14, the selectivity coefficient log *K* represents the different interactions that occur between the resin and the component. Changing the selectivity coefficient shifts the breakthrough curve. Smaller selectivity coefficients mean that the component breaks through faster from the

column. Therefore, lithium, cobalt and nickel have very low values because they do not interact with TP-260. Because metals like copper and aluminum interact with the resin much more, they have a higher log *K* value. These metals also tend to push less active metals out from the resin resulting in higher concentrations in the outlet feed compared to the feed solution. The *h* parameter describes the stoichiometry of the component attaching to the resin. It can be used to achieve different rates of exchange even when the activities are similar. The *h* parameter affects the width of the breakthrough profile, i.e. how narrow or broad is the transition from the initial state (usually zero concentration) to the final concentration (usually feed concentration). Because of this effect the *h* parameters of aluminum, manganese and copper are lower than 1 since their curves slope more gently. For nickel and cobalt, the parameter is changed because with just the selectivity coefficient, the model breaks all the early components at the same time. The mass transfer parameters can be used to affect the steepness of the breakthrough curves in the system as well as the moment when the breakthrough happens. Low mass transfer parameters mean that the breakpoint happens very early, but the component does not achieve the operational limit before the other components have already broken through. Because of this reason, the value is lowered for copper in order to achieve the very gentle slope the experimental data showcases.

After applying the parameters for the calculations, the process configuration, bed characteristics, calculation parameters and feed concentrations are given in ResSim. A simplistic version for one column operation is showcased in Figure 15.

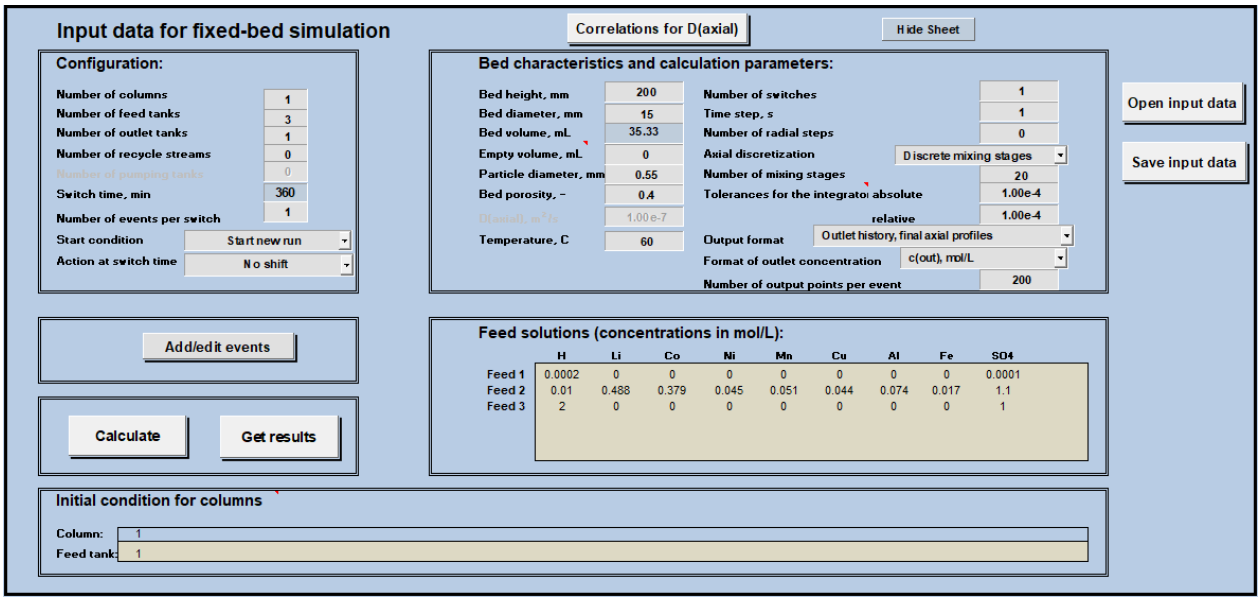

Figure 15. Process configuration for a simple fixed-bed column process for lithium ion battery leachate.

The events of the process are also required in this phase of simulation. The bed characteristics, temperature and pH are based on the laboratory experiments. For the initial parameter estimation, concentrations based on the experiments shown in 6.4 are used. The number of mixing stages is lowered to 20 because it decreases the time that each simulation takes drastically. There are three initial feeds consist of sulfuric acid as eluent (Feed 3), the lithium ion battery leachate (Feed 2) and water (Feed 1). These feed solutions play crucial parts in the events of the process. For the simplest of application, 4 different events were used. These include loading, washing, elution and washing. These can be seen in Figure 16.

Event table 39.62264151 Hide Sheet

Unit	Event 1	210	Event 2	90	Event 3	150	Event 4	90
	Length, min	210	Length, min	90	Length, min	150	Length, min	90
	Feed to/ outlet from column	Feed/outlet/ recycle rate, mL/min	Feed to/ outlet from column	Feed/outlet/ recycle rate, mL/min	Feed to/ outlet from column	Feed/outlet/ recycle rate, mL/min	Feed to/ outlet from column	Feed/outlet/ recycle rate, mL/min
Feed tank 1	1	0	1	1	1	0	1	1
Feed tank 2	1	1	1	0	1	0	1	0
Feed tank 3	1	0	1	0	1	1	1	0
Outlet tank 1	1	1	1	1	1	1	1	1
	Check configuration		Check configuration		Check configuration		Check configuration	

Figure 16. Event table for a complete process cycle.

7.3 Initial Ion Exchange Simulation Results

The number of parameters that needed to be estimated for a multicomponent system proved to be a challenging task. Having multiple components in the NICA model make them very delicate to the smallest changes. In contrast, the small changes have large effects on the entire system. Additional challenges arise from the fact that many of the components start breaking through at similar bed volumes. This can be seen in the laboratory experiments that can be seen in part 6.4 where most of the breakthroughs start in clusters.

7.3.1 Loading

When visually fitting simulation data with experimental results, the logical way is to attempt to simulate the breakthrough points for each metal individually. Copper and iron were the optimal metals to start fitting simulation data with the experimental results showcased in 6.4 because they had the longest breakthrough in the process. The early breakthrough metals such as cobalt are hard

to simulate initially since they do not attach themselves to the resin as hard. For this reason, even the slightest changes to the simulation parameters result in huge changes in the simulation results.

In the loading simulations, the presence of iron proved to be the hardest component because it has a high activity with the resin, attaching to it very aggressively. This had the effect that adding iron in the system pushed manganese and aluminum out of the resin sites. In addition to just pushing the previous metals from the resin, the presence of iron made it very hard to achieve similar steepness and curvature for aluminum and manganese. Because of the nature of the NICA model and the competitive ion exchange occurring in the system, the slightest changes for any parameter affected every other metal and their breakthroughs accordingly. Having a seven-component ion exchange process and knowing only the outlet concentrations of the experimental results made finding suitable parameters and fit between the simulated results and experimental data very difficult. The best results are showcased in Figures 17 and 18.

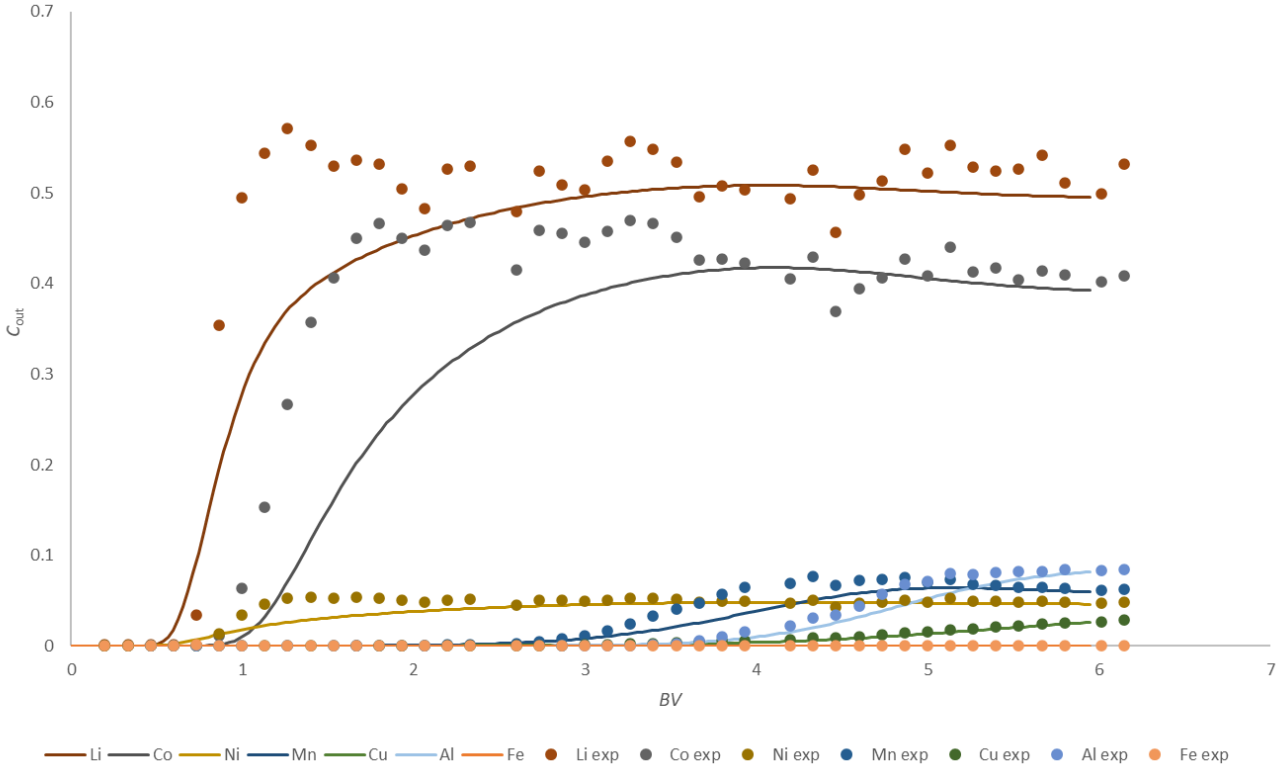

Figure 17. Simulated fixed-bed ion exchange in 60 ˚C and pH 2 results for lithium ion battery leachate. Lines represent simulated data.

Figure 17 showcases that especially for lithium and cobalt the simulated data cannot predict, how fast the actual breakthrough of the metals is in the system. The experimental data also showcases some fluctuation after breakthrough for cobalt and lithium. The simulated data is almost straight after breakthrough. However, when taking into account the difficult nature of the simulation task, the obtained fits were reasonably good.

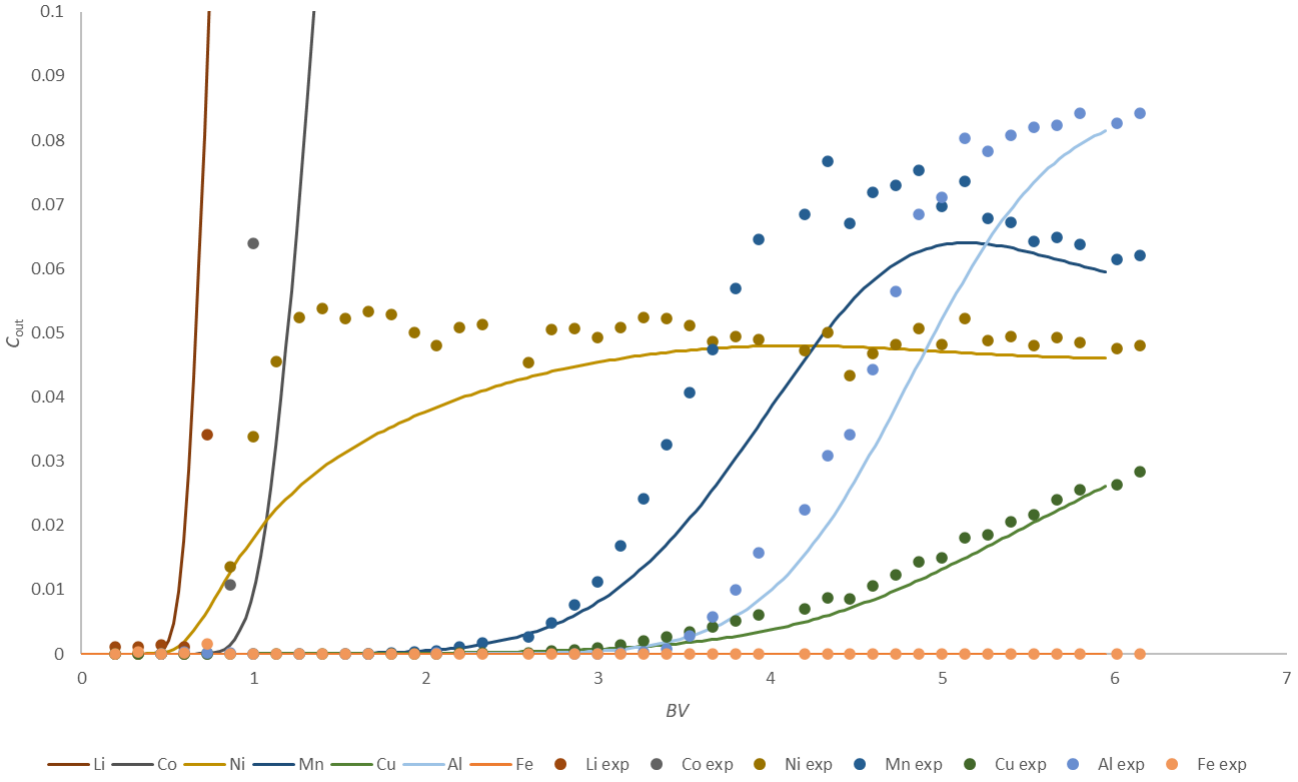

Figure 18. Simulated fixed-bed ion exchange in 60 ˚C and pH 2 results for lithium ion battery leachate focusing on nickel, manganese, aluminum, copper and iron.

Figure 18 showcases that it is possible to visually apply parameters that generate somewhat similar results when compared to the results in showcased in part 6.4. The simulated curves for iron, copper and aluminum are very similar to the experimental data. Aluminum breaks a little later in the

simulated data. Manganese starts breaking through at the same time in both simulated and experimental data. However, in the simulations the breakthrough happens much slower. For nickel the simulated results represent the experimental data poorly. Experimental data indicates that nickel breaks through very rapidly at 0.8 BV. In the simulated data nickel starts breaking through at 0.5 and achieves exhaustion point at 3.5 BV. This is a phenomenon that is common between every metal that has low affinity to the ion exchange resin.

Since the most prevalent metals in LIB leachate are lithium and cobalt, it is difficult to see from a single figure, how well the simulated data fits the experimental results. It is easier to assess the performance of the model using concentration ratios as was used in the experimental results showcased in 6.4. This was done in Figure 19.

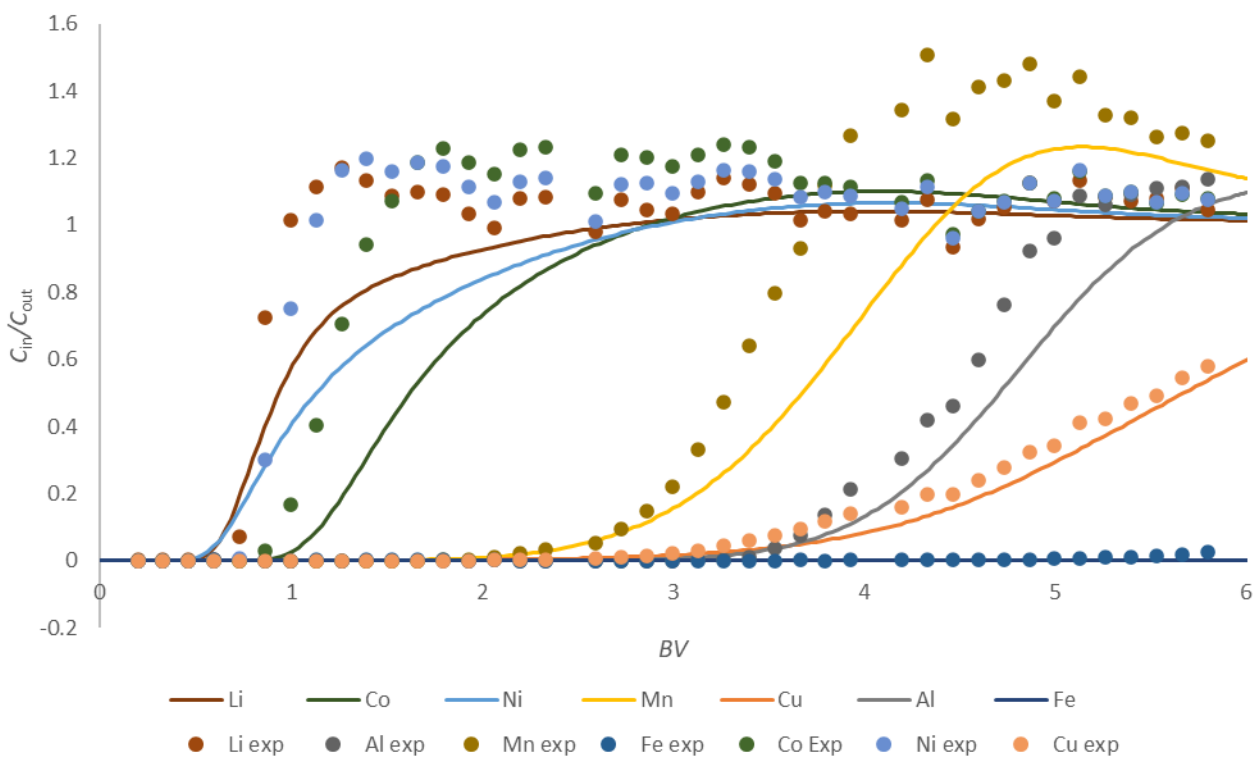

Figure 19. Combined breakthroughs from loading experiment showcased in 6.4 and simulations for the loading step in concentration ratios.

Figure 19 showcases that the breakthrough for lithium and nickel occurs sooner in the simulated model. In the experimental data, their outlet concentrations exceed their initial concentrations. However, the model cannot predict this behavior in the system. For manganese, the breakthrough starts at 2.5 BV in both cases. The simulations fail to predict the scale of the overshooting that happens for manganese in the experimental system due to interference from other metals pushing it out of the resin. This is possibly because the breakthrough of manganese occurs much slower in the simulated model. With aluminum and copper, the simulated breakthrough curves have good fit compared to the experimental data even with the presence of iron in the simulations pushing them out from the resin. Despite that inaccuracies the breakthroughs start around the same time in both simulated and experimental results. The simulations showcase that loading part of the ion exchange process can predict some phenomena occurring in the system and thus provide valuable information. However, the complexity of the system leaves noticeable inaccuracies in the simulated results especially on the speed of breakthrough for some components.

7.3.2 Loading Purity

The primarily considered impurity metals in the LIB leachate are manganese, aluminum, copper and iron. The primary objective of the ion exchange process is to remove these impurities effectively. The results seen in Figure 17 show that it is possible to separate the more valuable metals cobalt, nickel and lithium from the impurities. The obtained Li/Co/Ni raffinate is the desired result from the ion exchange process. However, copper and manganese have significant economic value, even though they are considered to be impurities. Because of the economic value, there may be significant benefits in separating copper and manganese from the rest of the impurities. The purity of the obtained raffinate from the loading was calculated with the concentrations of the metals in the simulated loading process. The results can be seen in Figure 20.

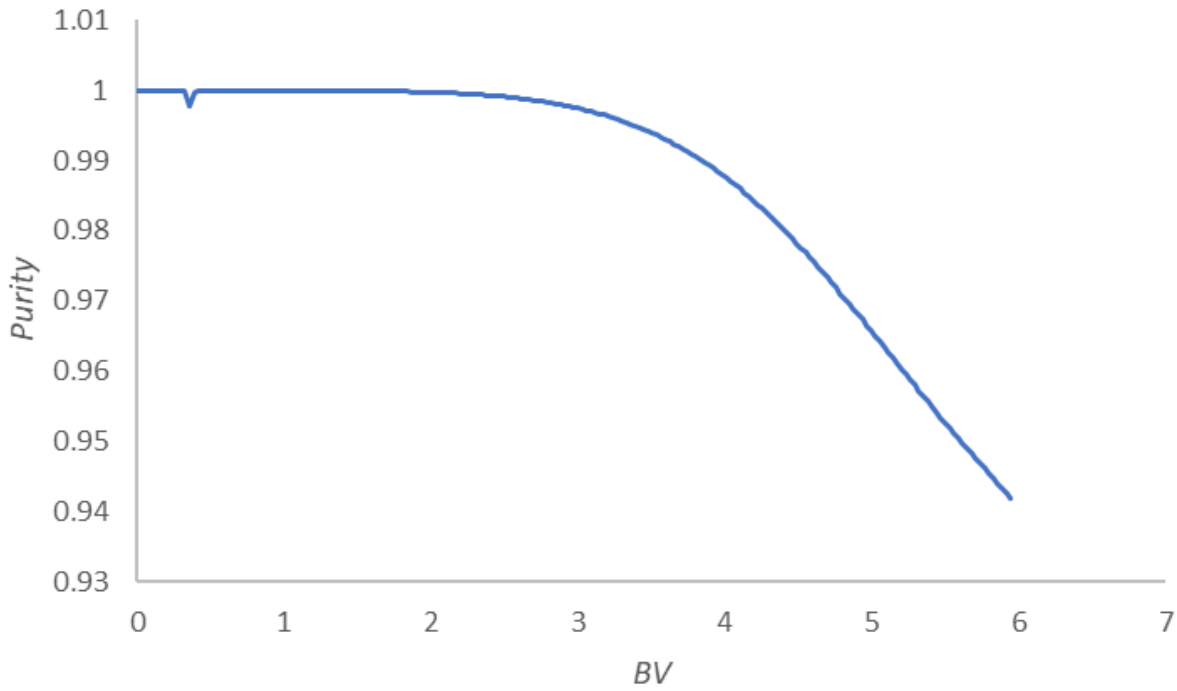

Figure 20. Purity of the solution gained from the simulated loading process.

Figure shows that even when the impurities are released from the resin the solution is still majorly comprised of valuable metals. This is mostly due to the abundance of lithium and cobalt compared to every other metal in the LIB leachate. If 99.5 % is taken as a threshold for good purity, the loading process reaches it at around 3.5 BV when manganese starts breaking through the column.

7.3.3 Elution

The experimental results presented in part 6.4 showed that except for aluminum and iron, every component can be removed from the resin with sulfuric acid. The simulations for the elution phase of the operation were done using the same operation conditions than the experimental results and

the same model parameters that were used in the loading step. The initial elution simulations can be seen in Figure 21.

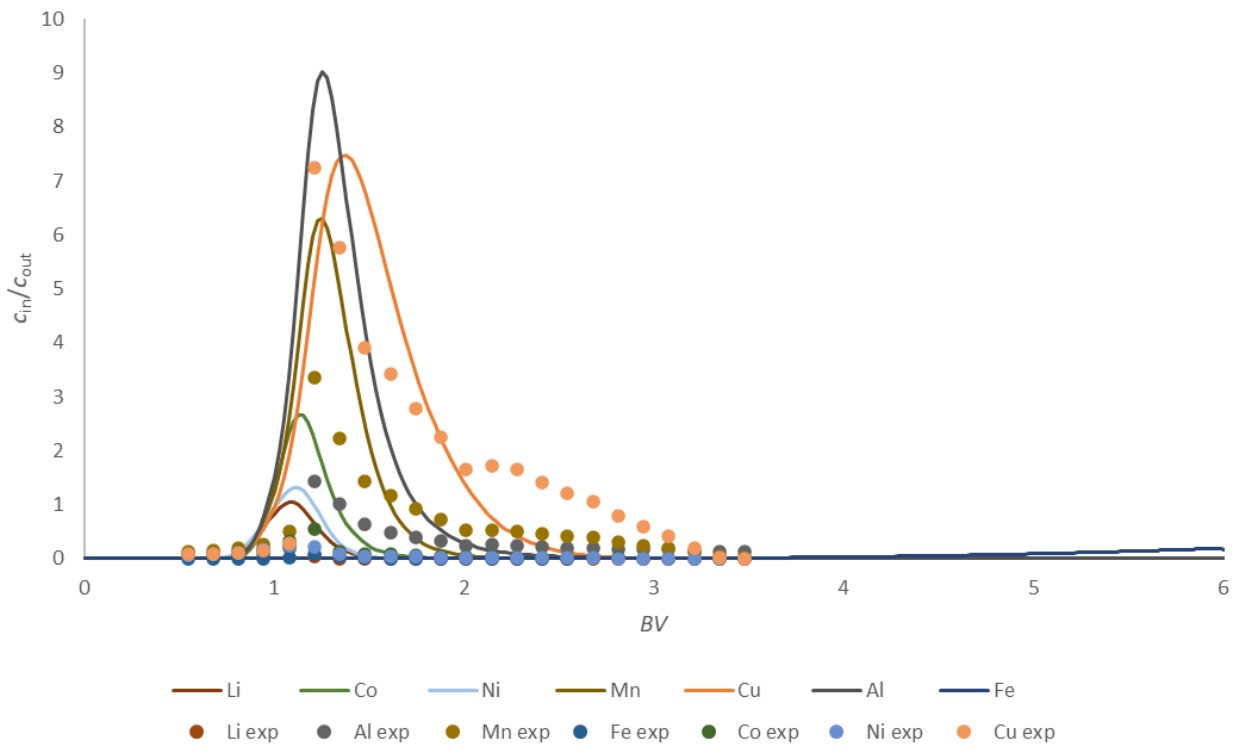

Figure 21. Simulated elution results excluding iron using 2 BV/h, 2 pH, 60 ˚C and 2M sulfuric acid as eluent.

It can be seen from Figure 21 that the elution curves are not similar in the same sense as the loading curves when simulation results are compared to laboratory experiments presented in 6.4. The elution spikes occur at 1 BV in the laboratory experiments and at around 0.8 BV in the simulations.

The simulation results have glaring errors in the concentrations. In the laboratory experiments, the elution rate for copper was faster. The concentrations were similar. In the experimental data, copper had a small spike at 2 BV. This is absent from the model. The biggest error is that based on the simulations, aluminum can be extracted from the system with sulfuric acid. However, the laboratory experiments showcase that iron and aluminum cannot be extracted by using sulfuric acid. The simulated model displays clear error for the behavior of aluminum in the system, making

the results unreliable. Manganese is removed in both the laboratory experiments and the simulations. It seems by looking at the results that the simulation model predicts higher yields of manganese than the experimental results. There are also inaccuracies for the metals that have low affinity to the resin. Nickel and lithium have spikes at concentration ratios of 1. For cobalt the inaccuracy is even larger spiking at 2.5 c_{in}/c_{out}.

The model inaccuracies regarding the elution step of the ion exchange process are problematic. It is not clear what causes the errors to manifest themselves in the model. The model is accurate in dynamic behavior. If the same parameters are utilized and the flowrate is increased, it results in faster elution times. The concentration spikes are also affected on, how strong the used eluent is. These results indicate that the model is either too complex to predict each component's behavior correctly, or the components themselves are not represented correctly in the simulation data.

There are trends that can be seen from the elution simulations. For every other metal than copper, the model seems to overestimate the effectiveness of sulfuric acid elution and its capabilities of stripping the components from the resin. For some metals the inaccuracies are more noticeable. For example, aluminum behaves completely different in the simulation data compared to experimental results. Observing this phenomenon gives insight on the possible problems that might surface when simulating complicated systems. Processes with multiple variable parameters and components may produce surprising results when simulated. This is a key concept for future applications, where complex processes are simulated. It also points out, why in some cases, simplification might be necessary to achieve better results.

7.4 Complete Operation Cycle

The simplest ion exchange process consists of at least 4 steps. These include 2 washing steps, a loading step and an elution step. The duration and the flowrates are based on previously conducted laboratory experiments (Kaukinen, 2019). The duration and flowrates for each step can be seen in Table 1, and the outlet concentrations for the whole cycle are represented in Figure 22.

Table 1. Steps, durations and flowrates for one complete ion exchange process cycle.

Step	Duration, BV	Flowrate, BV/h
Loading	6	2
Wash	2	6
Elution	4	2
Wash	2	6

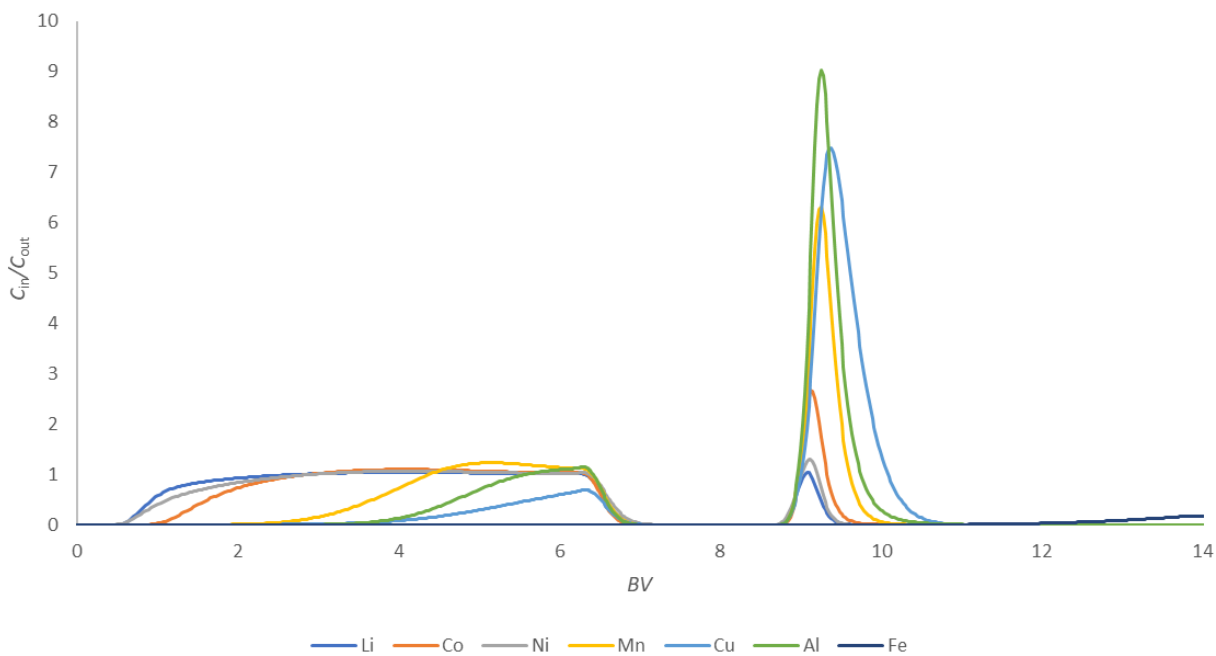

Figure 22. Simulated outlet concentrations of a complete ion exchange process cycle for a fixed-bed column. Process conditions were 2 BV/h, 2 pH, 60 ˚C and 2M sulfuric acid as eluent.

Each of the process steps can be seen clearly in Figure 22. The model works as planned when compared to the previous simulations. Loading is the first step and it ends at 7 BV when the water washing starts. From 7 to 8 BV the final inlet solution from the loading step come out from the

column. After the washing step, the elution step begins. Interestingly, it starts at around 9 BV. This is more like the actual laboratory results. The initial elution simulations using the same flowrate as the loading started already at 0.5 BV.

7.4.1 Second Cycle Performance

The simulation model seems to perform well with only four steps. When using sulfuric acid as the elution solution, it replaces the desired ions in the resin with hydrogen ions. Point of interest for the whole process is, how much does one complete cycle effect the capacities and results in the model. The need for regeneration, depends on, how well does the process keep a viable level of efficiency after each cycle. For this, a 2-cycle simulation was conducted with the same durations and flowrates as in the simulations seen in Figure 22. The results are seen in Figure 23.

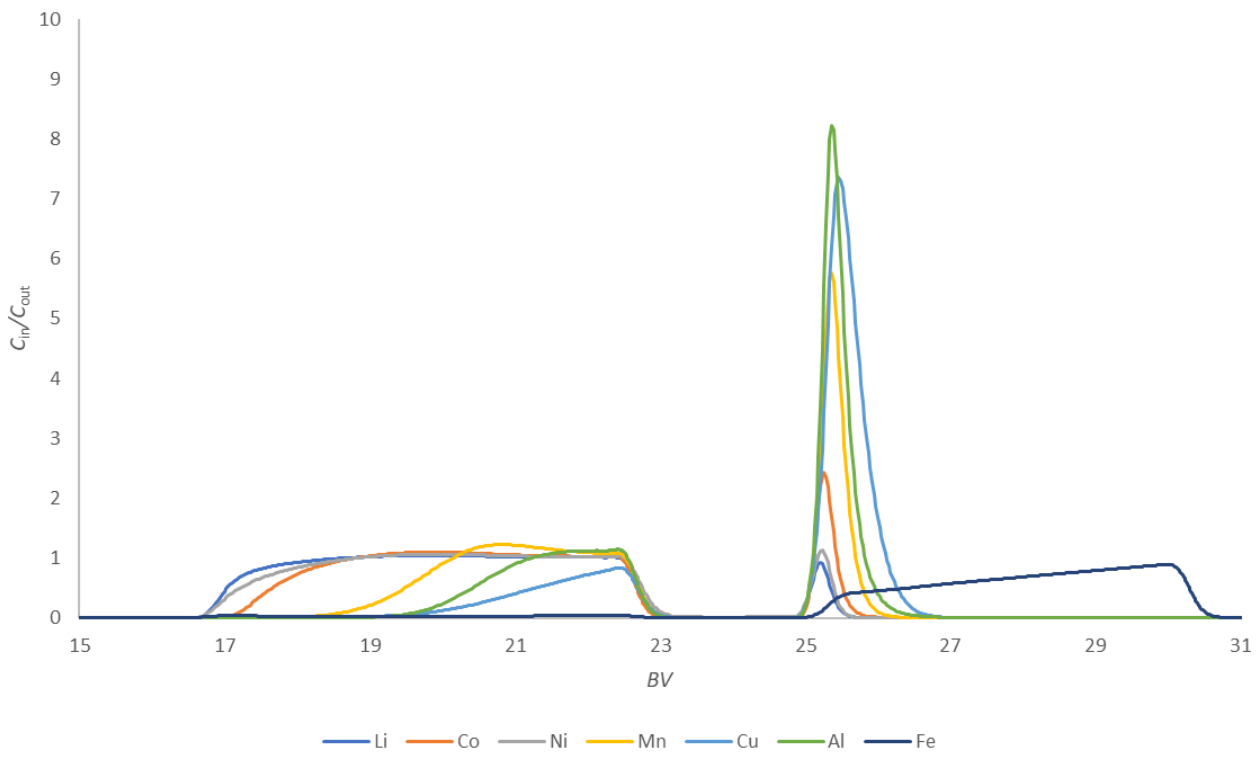

Figure 23. Simulated outlet concentrations of a second cycle for an ion exchange process. Process conditions were 2 BV/h, 2 pH, 60 ˚C and 2M sulfuric acid as eluent.

The results of the second cycle are somewhat similar to the curves displayed in Figure 22. However, some differences occur with the second cycle of steps. The amount of copper in the outlet stream in the loading stage increased in the second cycle. The amount of aluminum gained from elution has also decreased noticeably. The biggest difference is the behavior of iron in the second cycle. This might be due to the abundance of iron in the system since iron is not eluted with sulfuric acid. The first cycle in Figure 22. showcases that iron starts to elute very slowly at 12.5 BV. Because there is more leftover iron in the second cycle, this phenomenon occurs more intensely. In spite of this shortcoming, the elution phase of the second cycle gives valuable insight on how a possible simulation model behaves.

8 Future Considerations

The results shown in chapter 7 prove that even with a vast array of different mathematical models it is difficult to simulate complex ion exchange processes accurately. While it may be possible to accurately fit parameters visually, it is difficult to predict, how the generated model will behave in the entire process. This is well presented in the results showcased in chapter 7. While the simulated loading data represented the experimental data favorably, the model failed to model the elution process utilizing the same parameters as in the loading phase. This behavior showcases that simulating accurate process behavior for complex ion exchange processes, requires additional thought to just visually trying to fit simulation results to experimental concentration curves.

The largest obstacle for generating an accurate model was the large amount of different metals in the system. Because the behavior of the metal ions is preferably modelled as accurately as possible, it increases the number of phenomena that need to be considered. The NICA model presented in 4.7 was used due to its practical accuracy. However, coupling the highly accurate model with a process that has seven metal ions, protons and sulfate ions makes the number of parameters in the system very high. The large number of parameters and species in the system in addition to the ions competing for finite number of spaces on the resin, make the model very delicate to even the slightest changes to each parameter. Changing each parameter affects the whole system and every other ion in it. This makes visual parameter estimation very difficult to the point that simplifications may need to be considered. Either select a slightly less accurate model or reduce the amount of species in the process.

Another disadvantage for the parameter estimation was the low amount of experimental data available. Only the outlet concentrations for every metal as a function of bed volume were available. For example, the number of protons how their concentration in the loading phase developed proved to be crucial information that was lacking. In addition to just providing more data from the conducted experiments, additional selectivity or titration data could be used to fit parameters more accurately.

Even when the model failed to accurately represent the whole ion exchange process, the accurate results generated for the loading phase showcased promise. It shows that it is possible to produce accurate representations of ion exchange processes with more information of the whole process.

Since utilizing ion exchange with chelating resins for treating LIB leachate is a new concept, there was not any proved concept on how these kinds of processes should be simulated. Future attempts for generating a functional and accurate model should be easier based on the results of these experiments. Complete and accurate model can then be used to explore, how a complete applicable continuous process would behave. This would give precious insight on the efficiency of using ion exchange with chelating resins in larger scales.

9. Conclusions

The purpose of this thesis was to achieve an understanding of different types of methods for modeling battery metals ion exchange processes. The different types of models were studied to find the most suitable model for predicting behavior for an ion exchange process, where acid leachate from lithium-ion batteries was processed. This was done because valuable metals are present in these lithium-ion batteries. In addition to having economical value, there is pressure to find sustainable ways to recycle the materials used in lithium-ion batteries. Ion exchange has recently been studied as a suitable recycling process for lithium-ion batteries.

After valuating different types of methods for modelling ion exchange processes, non-ideal competitive adsorption NICA was selected. NICA is an accurate model for especially multicomponent ion exchange. NICA was then used to predict, how the different metal ions would move inside a fixed bed column filled with a chelating resin TP-260. This was done by visually adjusting the parameters in the NICA model according to previously obtained experimental data. Visually fitting the parameters for a process containing seven different metals proved to be very difficult. Even as the initial loading phase of the process was simulated accurately, the model failed to represent the experimental data in the elution phase.

The simulation data shows that it is possible to simulate even complex ion exchange processes with reasonable accuracy. However, the lack of different types of experimental data proved to be a massive drawback for the parameter estimation. The results also showcased that simulating complex processes is not as simple as just mimicking the operation conditions of actual experiments. Visually fitting the parameters to match experimental data proved to be largely trial and error. It is also the case that simulations can easily generate clear errors due to either the selected model or the simulation software being unable to cope with such complex systems. Even with all the shortcomings the results indicate that simulating the process accurately might be possible if the experimental data is provided with simulations in mind. Accurate simulations are powerful tools for gaining understanding, how different processes act in larger scales or how to optimize the process to yield most favorable results.

References

Aniceto, J.P.S., Cardoso, S.P., Faria, T.L., Lito, P.F., Silva, C.M., 2012. Modeling ion exchange equilibrium: Analysis of exchanger phase non-ideality. Desalination 290, 43–53. https://doi.org/10.1016/j.desal.2012.01.001

Borba, C.E., Silva, E.A., Spohr, S., Santos, G.H.F., Guirardello, R., 2011. Application of the mass action law to describe ion exchange equilibrium in a fixed-bed column. Chem. Eng. J. 172, 312–320. https://doi.org/10.1016/j.cej.2011.06.002

Carmona, M., Lucas, A.D., Valverde, J.L., Velasco, B., Rodríguez, J.F., 2006. Combined adsorption and ion exchange equilibrium of phenol on Amberlite IRA-420. Chem. Eng. J. 117, 155–160. https://doi.org/10.1016/j.cej.2005.12.013

Chagnes, A., Pospiech, B., 2013. A brief review on hydrometallurgical technologies for recycling spent lithium-ion batteries. J. Chem. Technol. Biotechnol. 88, 1191–1199. https://doi.org/10.1002/jctb.4053

Chen, X., Chen, Y., Zhou, T., Liu, D., Hu, H., Fan, S., 2015. Hydrometallurgical recovery of metal values from sulfuric acid leaching liquor of spent lithium-ion batteries. Waste Manag. 38, 349–356. https://doi.org/10.1016/j.wasman.2014.12.023

Chowdhury, Z., Abd Hamid, S.B., Zain, S., 2014. Evaluating Design Parameters for Breakthrough Curve Analysis and Kinetics of Fixed Bed Columns for Cu(II) Cations Using Lignocellulosic Wastes. BioResources 10. https://doi.org/10.15376/biores.10.1.732-749

Chowdiah, V., Foutch, G.L., 2002. A Kinetic Model for Cationic-Exchange-Resin Regeneration [WWW Document]. https://doi.org/10.1021/ie00038a045

Costa, J.F. de S.S., Vilar, V.J.P., Botelho, C.M.S., da Silva, E.A.B., Boaventura, R.A.R., 2010. Application of the Nernst–Planck approach to lead ion exchange in Ca-loaded Pelvetia canaliculata. Water Res. 44, 3946–3958. https://doi.org/10.1016/j.watres.2010.04.033

Dranoff, J., Lapidus, L., 1957. Equilibrium in Ternary Ion Exchange Systems [WWW Document]. https://doi.org/10.1021/ie50572a038

Dreyer, W., Guhlke, C., Müller, R., 2013. Overcoming the shortcomings of the Nernst–Planck model. Phys. Chem. Chem. Phys. 15, 7075–7086. https://doi.org/10.1039/C3CP44390F

Gaines, L., 2018. Lithium-ion battery recycling processes: Research towards a sustainable course. Sustain. Mater. Technol. 17, e00068. https://doi.org/10.1016/j.susmat.2018.e00068

Gao, W., Song, J., Cao, H., Lin, X., Zhang, X., Zheng, X., Zhang, Y., Sun, Z., 2018. Selective recovery of valuable metals from spent lithium-ion batteries – Process development and kinetics evaluation. J. Clean. Prod. 178, 833–845. https://doi.org/10.1016/j.jclepro.2018.01.040

Georgi-Maschler, T., Friedrich, B., Weyhe, R., Heegn, H., Rutz, M., 2012. Development of a recycling process for Li-ion batteries. J. Power Sources 207, 173–182. https://doi.org/10.1016/j.jpowsour.2012.01.152

Golmohammadzadeh, R., Rashchi, F., Vahidi, E., 2017. Recovery of lithium and cobalt from spent lithium-ion batteries using organic acids: Process optimization and kinetic aspects. Waste Manag. 64, 244–254. https://doi.org/10.1016/j.wasman.2017.03.037

Guo, Y., Li, F., Zhu, H., Li, G., Huang, J., He, W., 2016. Leaching lithium from the anode electrode materials of spent lithium-ion batteries by hydrochloric acid (HCl). Waste Manag. 51, 227–233. https://doi.org/10.1016/j.wasman.2015.11.036

Helfferich, F.G., 1995. Ion Exchange. Courier Corporation.

Höll, W.H., Horst, J., 1997. Application of the Surface Complex Formation Model to Ion Exchange Equilibria. J. Colloid Interface Sci. 195, 250–260. https://doi.org/10.1006/jcis.1997.5170

Holopainen, O., 2016. Kuparin poistaminen vesiliuoksesta ioninvaihdolla. Removing copper from aqueous solution by ion exchange.

Inglezakis, V.J., Zorpas, A., 2012. Fundamentals of Ion Exchange Fixed-Bed Operations, in: Dr., I., Luqman, M. (Eds.), Ion Exchange Technology I: Theory and Materials. Springer Netherlands, Dordrecht, pp. 121–161. https://doi.org/10.1007/978-94-007-1700-8_4

Ioannidis, S., Anderko, A., Sanders, S.J., 2000. Internally consistent representation of binary ion exchange equilibria. Chem. Eng. Sci. 55, 2687–2698. https://doi.org/10.1016/S0009-2509(99)00540-0

Jeon, C., Höll, W.H., 2004. Application of the surface complexation model to heavy metal sorption equilibria onto aminated chitosan. Hydrometallurgy 71, 421–428. https://doi.org/10.1016/S0304-386X(03)00118-X

Kaukinen, A., 2019. Ion exchange in hydrometallurgical recycling of Li-ion battery metals : production of Li-Ni-Co mixture. Ioninvaihto hydrometallurgisessa Li-ioniakkumetallien kierrätyksessä : Li-Ni-Co seoksen valmistus.

Kim, H.T., Frederick, W.J., 1988. Evaluation of Pitzer ion interaction parameters of aqueous electrolytes at 25.degree.C. 1. Single salt parameters. J. Chem. Eng. Data 33, 177–184. https://doi.org/10.1021/je00052a035

Kinniburgh, D.G., Barker, J.A., Whitfield, M., 1983. A comparison of some simple adsorption isotherms for describing divalent cation adsorption by ferrihydrite. J. Colloid Interface Sci. 95, 370–384. https://doi.org/10.1016/0021-9797(83)90197-2

Kinniburgh, D.G., Milne, C.J., Benedetti, M.F., Pinheiro, J.P., Filius, J., Koopal, L.K., Van Riemsdijk, W.H., 1996. Metal Ion Binding by Humic Acid: Application of the NICA-Donnan Model. Environ. Sci. Technol. 30, 1687–1698. https://doi.org/10.1021/es950695h

Kinniburgh, D.G., van Riemsdijk, W.H., Koopal, L.K., Borkovec, M., Benedetti, M.F., Avena, M.J., 1999. Ion binding to natural organic matter: competition, heterogeneity, stoichiometry and thermodynamic consistency. Colloids Surf. Physicochem. Eng. Asp. 151, 147–166. https://doi.org/10.1016/S0927-7757(98)00637-2

Kónya, J., Nagy, N.M., 2013. Misleading information on homogeneity and heterogeneity obtained from sorption isotherms. Adsorption 19, 701–707. https://doi.org/10.1007/s10450-013-9495-6

Koopal, L.K., Saito, T., Pinheiro, J.P., Riemsdijk, W.H. van, 2005. Ion binding to natural organic matter: General considerations and the NICA–Donnan model. Colloids Surf. Physicochem. Eng. Asp., A Selection of Papers from the Third International Conference “Interfaces against Pollutions” (IAP 2004), May 24-27, Jülich, Germany 265, 40–54. https://doi.org/10.1016/j.colsurfa.2004.11.050

Krishna, R., Wesselingh, J.A., 1997. The Maxwell-Stefan approach to mass transfer. Chem. Eng. Sci. 52, 861–911. https://doi.org/10.1016/S0009-2509(96)00458-7

Ku, H., Jung, Y., Jo, M., Park, S., Kim, S., Yang, D., Rhee, K., An, E.-M., Sohn, J., Kwon, K., 2016. Recycling of spent lithium-ion battery cathode materials by ammoniacal leaching. J. Hazard. Mater. 313, 138–146. https://doi.org/10.1016/j.jhazmat.2016.03.062

Kumar, K.V., Castro, M.M. de, Martinez-Escandell, M., Molina-Sabio, M., Rodriguez-Reinoso, F., 2010. A Continuous Binding Site Affinity Distribution Function from the Freundlich Isotherm for the Supercritical Adsorption of Hydrogen on Activated Carbon [WWW Document]. https://doi.org/10.1021/jp104014f

Kushnir, D., 2015. Lithium Ion Battery Recycling Technology 2015 56.

Laatikainen, K., Laatikainen, M., Branger, C., Paatero, E., Sirén, H., 2012. Role of Ligand Acidity in Chelating Adsorption and Desorption of Metal Salts. Ind. Eng. Chem. Res. 51, 12310–12320. https://doi.org/10.1021/ie301115u

Laatikainen, M., 2014. ResMod Toolbox for Parameter Estimation and Process Simulation in Ion Exchange and Adsorption.

Laatikainen, M., 2011. Modeling of electrolyte sorption – from phase equilibria to dynamic separation systems. Lappeenranta University of Technology.

Laatikainen, M., Laatikainen, K., 2016. Chelating adsorption with variable stoichiometry: Separation of nickel and zinc in concentrated sulfate solution. Chem. Eng. J. 287, 74–82. https://doi.org/10.1016/j.cej.2015.11.036

Lewatit-TP-260-L.pdf [WWW Document], 2020. URL https://www.lenntech.com/Data-sheets/Lewatit-TP-260-L.pdf (accessed 11.2.20).

Li, H., Xing, S., Liu, Y., Li, F., Guo, H., Kuang, G., 2017. Recovery of Lithium, Iron, and Phosphorus from Spent LiFePO4 Batteries Using Stoichiometric Sulfuric Acid Leaching System. ACS Sustain. Chem. Eng. 5, 8017–8024. https://doi.org/10.1021/acssuschemeng.7b01594

Li, X., Mu, W., Xiang, X., Liu, B., Tang, H., Zhou, G., Wei, H., Jian, Y., Luo, S., 2014. Strontium adsorption on tantalum-doped hexagonal tungsten oxide. J. Hazard. Mater. 264, 386–394. https://doi.org/10.1016/j.jhazmat.2013.11.032

Li, Y.-S., Dong, Y.-L., 2004. Determination of anion-exchange resin performance based on facile chloride-ion monitoring by FIA-spectrophotometry with applications to water treatment operation. Anal. Sci. Int. J. Jpn. Soc. Anal. Chem. 20, 831–836. https://doi.org/10.2116/analsci.20.831

Lin, H., Tang, Y., Liu, T., Matsuyama, H., Wang, X., 2016. Understanding the thermally induced phase separation process via a Maxwell–Stefan model. J. Membr. Sci. 507, 143–153. https://doi.org/10.1016/j.memsci.2016.01.049

Lito, P.F., Cardoso, S.P., Loureiro, J.M., Silva, C.M., 2012. Ion Exchange Equilibria and Kinetics, in: Dr., I., Luqman, M. (Eds.), Ion Exchange Technology I: Theory and Materials. Springer Netherlands, Dordrecht, pp. 51–120. https://doi.org/10.1007/978-94-007-1700-8_3

London Metal Exchange: Home [WWW Document], 2020. URL https://www.lme.com/ (accessed 5.18.20).

Lopes, C.B., Lito, P.F., Cardoso, S.P., Pereira, E., Duarte, A.C., Silva, C.M., 2012. Metal Recovery, Separation and/or Pre-concentration, in: Inamuddin, Dr., Luqman, M. (Eds.), Ion Exchange Technology II: Applications. Springer Netherlands, Dordrecht, pp. 237–322. https://doi.org/10.1007/978-94-007-4026-6_11

Marinsky, J.A., 1996. Alternate Interpretation of the Change Observed in H+ Ion Concentration Levels of the Aqueous Medium of Metal Oxide Suspensions in Response to Change in the Electrolyte Concentration Levels of the Aqueous Medium [WWW Document]. https://doi.org/10.1021/jp952274s

Melis, S., Markos, J., Cao, G., Morbidelli, M., 1996. Multicomponent equilibria on ion-exchange resins. Fluid Phase Equilibria, Proceedings of the Seventh International Conference on Fluid Properties and Phase Equilibria for Chemical Process Design 117, 281–288. https://doi.org/10.1016/0378-3812(95)02964-8

Nasef, M.M., Ujang, Z., 2012. Introduction to Ion Exchange Processes, in: Dr., I., Luqman, M. (Eds.), Ion Exchange Technology I: Theory and Materials. Springer Netherlands, Dordrecht, pp. 1–39. https://doi.org/10.1007/978-94-007-1700-8_1

Pagnanelli, F., Moscardini, E., Altimari, P., Abo Atia, T., Toro, L., 2017. Leaching of electrodic powders from lithium ion batteries: Optimization of operating conditions and effect of physical pretreatment for waste fraction retrieval. Waste Manag., Special Thematic Issue: Urban Mining and Circular Economy 60, 706–715. https://doi.org/10.1016/j.wasman.2016.11.037

Petrus, R., Warchoł, J.K., 2005. Heavy metal removal by clinoptilolite. An equilibrium study in multi-component systems. Water Res. 39, 819–830. https://doi.org/10.1016/j.watres.2004.12.003

Pitzer, K.S. (Ed.), 1991. Activity coefficients in electrolyte solutions, 2nd ed. ed. CRC Press, Boca Raton.

Pitzer, K.S., 1973. Thermodynamics of electrolytes. I. Theoretical basis and general equations. J. Phys. Chem. 77, 268–277. https://doi.org/10.1021/j100621a026

Plazinski, W., 2013. Equilibrium and kinetic modeling of metal ion biosorption: on the ways of model generalization for the case of multicomponent systems. Adsorption 19, 659–666. https://doi.org/10.1007/s10450-013-9489-4

Porvali, A., Aaltonen, M., Ojanen, S., Velazquez-Martinez, O., Eronen, E., Liu, F., Wilson, B.P., Serna-Guerrero, R., Lundström, M., 2019. Mechanical and hydrometallurgical processes in HCl media for the recycling of valuable metals from Li-ion battery waste. Resour. Conserv. Recycl. 142, 257–266. https://doi.org/10.1016/j.resconrec.2018.11.023

Provis, J.L., Lukey, G.C., Shallcross, D.C., 2005. Modeling Multicomponent Ion Exchange: Application of the Single-Parameter Binary System Model. Ind. Eng. Chem. Res. 44, 2250–2257. https://doi.org/10.1021/ie049197k

Putro, J.N., Santoso, S.P., Ismadji, S., Ju, Y.-H., 2017. Investigation of heavy metal adsorption in binary system by nanocrystalline cellulose – Bentonite nanocomposite: Improvement on extended Langmuir isotherm model. Microporous Mesoporous Mater. 246, 166–177. https://doi.org/10.1016/j.micromeso.2017.03.032

Qamar, S., Nawaz Abbasi, J., Javeed, S., Seidel-Morgenstern, A., 2014. Analytical solutions and moment analysis of general rate model for linear liquid chromatography. Chem. Eng. Sci. 107, 192–205. https://doi.org/10.1016/j.ces.2013.12.019

Sirola, K., Laatikainen, M., Lahtinen, M., Paatero, E., 2008. Removal of copper and nickel from concentrated ZnSO4 solutions with silica-supported chelating adsorbents. Sep. Purif. Technol. 64, 88–100. https://doi.org/10.1016/j.seppur.2008.08.001

Soldatov, V.S., 1995. Application of basic concepts of chemical thermodynamics to ion exchange equilibria. React. Funct. Polym., Proceedings of the Workshop on Uniform and Reliable Formulations Nomenclature and Experimentation for Ion Exchange 27, 95–106. https://doi.org/10.1016/1381-5148(95)00040-M

Stöhr, C., Horst, J., Höll, W.H., 2001. Application of the surface complex formation model to ion exchange equilibria: Part V. Adsorption of heavy metal salts onto weakly basic anion exchangers. React. Funct. Polym. 49, 117–132. https://doi.org/10.1016/S1381-5148(01)00067-0

Sud, D., 2012. Chelating Ion Exchangers: Theory and Applications, in: Dr., I., Luqman, M. (Eds.), Ion Exchange Technology I: Theory and Materials. Springer Netherlands, Dordrecht, pp. 373–401. https://doi.org/10.1007/978-94-007-1700-8_10

van Riemsduk, W.H., de Wit, J.C.M., Mous, S.L.J., Koopal, L.K., Kinniburgh, D.G., 1996. An Analytical Isotherm Equation (CONICA) for Nonideal Mono- and Bidentate Competitive Ion Adsorption to Heterogeneous Surfaces. J. Colloid Interface Sci. 183, 35–50. https://doi.org/10.1006/jcis.1996.0516

Virolainen, S., Suppula, I., Sainio, T., 2014. Continuous ion exchange for hydrometallurgy: Purification of Ag(I)–NaCl from divalent metals with aminomethylphosphonic resin using counter-current and cross-current operation. Hydrometallurgy 142, 84–93. https://doi.org/10.1016/j.hydromet.2013.11.012

Vo, B.S., Shallcross, D.C., 2005. Modeling Solution Phase Behavior in Multicomponent Ion Exchange Equilibria Involving H+, Na+, K+, Mg2+, and Ca2+ Ions. J. Chem. Eng. Data 50, 1995–2002. https://doi.org/10.1021/je050232j

Vo, B.S., Shallcross, D.C., 2003. Multi-Component Ion Exchange Equilibria Prediction. Chem. Eng. Res. Des., Separation Processes 81, 1311–1322. https://doi.org/10.1205/026387603771339528

Wang, M., Zhang, Y., Muhammed, M., 1997. Critical evaluation of thermodynamics of complex formation of metal ions in aqueous solutions I. A description of evaluation methods. Hydrometallurgy 45, 21–36. https://doi.org/10.1016/S0304-386X(96)00072-2

Warchoł, J., Petrus, R., 2006. Modeling of heavy metal removal dynamics in clinoptilolite packed beds. Microporous Mesoporous Mater. 93, 29–39. https://doi.org/10.1016/j.micromeso.2006.01.021

Xiong, Y., 2006. Estimation of medium effects on equilibrium constants in moderate and high ionic strength solutions at elevated temperatures by using specific interaction theory (SIT): Interaction coefficients involving Cl, OH- and Ac-up to 200°C and 400 bars. Geochem. Trans. 7, 4. https://doi.org/10.1186/1467-4866-7-4

Zhang, X., Xie, Y., Lin, X., Li, H., Cao, H., 2013. An overview on the processes and technologies for recycling cathodic active materials from spent lithium-ion batteries. J. Mater. Cycles Waste Manag. Dordr. 15, 420–430. http://dx.doi.org.ezproxy.cc.lut.fi/10.1007/s10163-013-0140-y